Kinetochore Biorientation in *Saccharomyces cerevisiae* Requires a Tightly Folded Conformation of the Ndc80 Complex

Jerry F. Tien,*,[1] Neil T. Umbreit,*,[2] Alex Zelter,* Michael Riffle,*,† Michael R. Hoopmann,‡ Richard S. Johnson,† Bryan R. Fonslow,§ John R. Yates, III,§ Michael J. MacCoss,† Robert L. Moritz,‡ Charles L. Asbury, and Trisha N. Davis*,[3]**

*Department of Biochemistry, †Department of Genome Sciences, and **Department of Physiology and Biophysics, University of Washington, Seattle, Washington 98195, ‡Institute for Systems Biology, Seattle, Washington 98109, and §Department of Chemical Physiology, The Scripps Research Institute, La Jolla, California 92037

ABSTRACT Accurate transmission of genetic material relies on the coupling of chromosomes to spindle microtubules by kinetochores. These linkages are regulated by the conserved Aurora B/Ipl1 kinase to ensure that sister chromatids are properly attached to spindle microtubules. Kinetochore–microtubule attachments require the essential Ndc80 complex, which contains two globular ends linked by large coiled-coil domains. In this study, we isolated a novel *ndc80* mutant in *Saccharomyces cerevisiae* that contains mutations in the coiled-coil domain. This *ndc80* mutant accumulates erroneous kinetochore–microtubule attachments, resulting in misalignment of kinetochores on the mitotic spindle. Genetic analyses with suppressors of the *ndc80* mutant and *in vitro* cross-linking experiments suggest that the kinetochore misalignment *in vivo* stems from a defect in the ability of the Ndc80 complex to stably fold at a hinge in the coiled coil. Previous studies proposed that the Ndc80 complex can exist in multiple conformations: elongated during metaphase and bent during anaphase. However, the distinct functions of individual conformations *in vivo* are unknown. Here, our analysis revealed a tightly folded conformation of the Ndc80 complex that is likely required early in mitosis. This conformation is mediated by a direct, intracomplex interaction and involves a greater degree of folding than the bent form of the complex at anaphase. Furthermore, our results suggest that this conformation is functionally important *in vivo* for efficient error correction by Aurora B/Ipl1 and, consequently, to ensure proper kinetochore alignment early in mitosis.

KINETOCHORES mediate the linkage between chromosomes and spindle microtubules during mitosis. This attachment is highly regulated to promote the fidelity of chromosome segregation. At metaphase, replicated chromosomes are attached to microtubules emanating from opposite poles, in a "bioriented" alignment. This ensures that each daughter cell receives a full complement of genetic material after chromosome segregation. Errors can occur in the form of "syntelic" attachments, when both sister kinetochores attach to microtubules emanating from the same pole. These erroneous kinetochore–microtubule attachments are detected and detached by the conserved Aurora B/Ipl1 kinase (Biggins *et al.* 2001; Biggins and Murray 2001; Tanaka *et al.* 2002; Pinsky *et al.* 2006). In the current prevailing model, Aurora B/Ipl1 corrects syntelic attachments by destabilizing linkages that are under low levels of tension (Nicklas and Koch 1969; Biggins and Murray 2001; Tanaka *et al.* 2002; Liu *et al.* 2009; Cane *et al.* 2013). The Aurora B/Ipl1 error detection system is coupled to the spindle checkpoint, a separate surveillance system that delays anaphase until all kinetochores are attached to spindle microtubules (reviewed in Hauf 2013). Together, these systems ensure that the physical separation of replicated chromatids does not occur until all kinetochore–microtubule attachments are bioriented.

The attachment of spindle microtubules to kinetochores requires the conserved Ndc80 complex (Figure 1A), a flexible

doi: 10.1534/genetics.114.167775
Manuscript received June 26, 2014; accepted for publication September 14, 2014; published Early Online September 16, 2014.
Supporting information is available online at http://www.genetics.org/lookup/suppl/doi:10.1534/genetics.114.167775/-/DC1.
[1]Present address: Michael Smith Genome Sciences Centre, British Columbia Cancer Agency, Vancouver, British Columbia, Canada V5Z 1L3.
[2]Present address: Department of Pediatric Oncology, Dana-Farber Cancer Institute, Boston, MA 02215.
[3]Corresponding author: Box 357350, Department of Biochemistry, University of Washington, Seattle, WA 98195. E-mail: tdavis@uw.edu

rod-shaped heterotetramer composed of Ndc80, Nuf2, Spc24, and Spc25 (Osborne *et al.* 1994; Janke *et al.* 2001; Wigge and Kilmartin 2001; Wei *et al.* 2005; Ciferri *et al.* 2008; Wang *et al.* 2008). The Ndc80 complex has a well-characterized role in microtubule binding, mediated by N-terminal calponin homology domains (Wei *et al.* 2007; Powers *et al.* 2009; Alushin *et al.* 2010). At the other end of the complex, the globular domains of Spc24 and Spc25 link the Ndc80 complex to other kinetochore components (De Wulf *et al.* 2003; Malvezzi *et al.* 2013; Nishino *et al.* 2013). Between the two structurally defined ends, the Ndc80 complex is composed of predicted coiled-coil domains from all four components (Wei *et al.* 2005; Wang *et al.* 2008). The coiled-coil domains are interrupted by a disordered "loop" region that is thought to enable flexion of the complex, as observed for recombinant Ndc80 complexes on negative-stain electron micrographs (Wang *et al.* 2008). The Ndc80 complex adopts elongated and bent conformations *in vivo* during metaphase and anaphase, respectively (Joglekar *et al.* 2009; Aravamudhan *et al.* 2014). However, it remains to be determined if these conformations arise from the flexibility of the complex at the loop observed *in vitro*. Furthermore, no previous study has examined whether the bending flexibility of the Ndc80 complex is important *in vivo*.

Our recent results from a mutagenesis screen suggest that several small regions of the coiled coil are essential for cell viability, including one region near the predicted loop (Tien *et al.* 2013). Here, biochemical characterization of the Ndc80 complex was combined with genetic analysis of a novel *ndc80* mutant to reveal that the loop region acts as a hinge *in vivo*, enabling the complex to adopt a tightly folded conformation. This conformation is mediated by a direct, intra-complex interaction between two regions of the complex on either side of the loop. Mutations in one of these regions impede the ability of Aurora B/Ipl1 to correct aberrant kinetochore–microtubule attachments prior to metaphase. Therefore, the tightly folded conformation of the Ndc80 complex is likely required to promote kinetochore biorientation early in mitosis.

Materials and Methods

Strains

All strains used in this study (Supporting Information, Table S1) were derived from W303.

Protein expression and purification

Recombinant *Saccharomyces cerevisiae* Ndc80 complex was expressed from two dicistronic plasmids (encoding Ndc80/Nuf2 and His_6-Spc24/Spc25) and purified as previously described (Wei *et al.* 2005; Powers *et al.* 2009).

Immunoprecipitation

For immunoprecipitation of Nuf2-TAP from *ndc80-121* cultures, 2 liters of JTY30-1A (*ndc80-121 NUF2-TAP*) cells were grown to ~100 Klett units in YPD at 25°. JTY30-4A (*NDC80 NUF2-TAP*) cells served as a wild-type control. Cultures were shifted to 37° for 100 min and harvested by centrifugation. Pellets were cryogenically ground into cell dust using a PM100 (Retsch) and stored at −80°, as per the protocol from the Rout laboratory (http://lab.rockefeller.edu/rout/assets/file/protocols). For each condition, 4 g of cell dust were resuspended in lysis buffer (20 mM HEPES, pH 7.4, 300 mM NaCl, 100 μM GTP, 1 mM MgCl2, 1 mM dithiothreitol, 4 $\mu g \cdot ml^{-1}$ pepstatin, 4 $\mu g \cdot ml^{-1}$ leupeptin, 4 $\mu g \cdot ml^{-1}$ aprotinin, 4 $\mu g \cdot ml^{-1}$ chymostatin, 1 mM phenylmethanesulfonyl fluoride, 1 mM sodium pyrophosphate, 1 mM sodium fluoride, 1 mM β-glycerophosphate, 5% glycerol, and 0.5% Triton X-100), homogenized, and cleared by centrifugation at 2000 × *g* for 10 min at 4°. An aliquot (250 μl) of 60 $mg \cdot ml^{-1}$ Dynabeads (Invitrogen) conjugated with rabbit IgG (MP Biomedicals) was added to the clarified lysate and incubated for 30 min at 4°. Beads were then washed three times with 150 μl of wash buffer (20 mM HEPES, pH 7.4, 200 mM NaCl, 100 μM GTP, 1 mM $MgCl_2$, 1 mM dithiothreitol, 4 $\mu g \cdot ml^{-1}$ pepstatin, 4 $\mu g \cdot ml^{-1}$ leupeptin, 4 $\mu g \cdot ml^{-1}$ aprotinin, 4 $\mu g \cdot ml^{-1}$ chymostatin, 1 mM phenylmethanesulfonyl fluoride, 1 mM sodium pyrophosphate, 1 mM sodium fluoride, 1 mM β-glycerophosphate, and 5% glycerol), washed once with 150 μl of Tobacco Etch Virus (TEV) buffer (40 mM HEPES, pH 7.4, 200 mM NaCl, 2 mM $MgCl_2$, 1 mM EDTA, 1 mM dithiothreitol, 1 mM GTP, and 5% glycerol), and resuspended in 100 μl TEV buffer. TEV was added to 67 nM and the reaction was incubated for 2 hr at 4°. Trichloroacetic acid protein precipitation was performed on 60 μl of eluate after TEV cleavage. Immunoprecipitated proteins were identified by mass spectrometry and MudPIT analysis.

Fluorescence microscopy

The CellAsic ONIX microfluidics system (Millipore) was used for time-lapse imaging of synchronized cells. For G1 synchronization, *MAT***a** cells (Table S1) were grown to ~60 Klett units at 25° and arrested for a total of 1.5 generations with α-factor. One generation into the arrest, cells were briefly sonicated and 50 μl were loaded onto an Y04C CellAsic ONIX plate. The arrest was completed on the plate before releasing into media lacking α-factor. For metaphase arrests, cells with an auxin-inducible Cdc20 degron (Table S1) were grown to ~50 Klett units at 25°, arrested with 500 μM 3-indoleacetic acid (Sigma-Aldrich) for 3 hr, and loaded onto a Y04C plate. All flow rates were at ~12 $\mu l \cdot hr^{-1}$. After completing the arrests, plate and objective heaters were raised to 37° (t = 0) and cells were imaged. Time-lapse images of cells were taken at 7.5-min intervals, with three z-sections spanning 2.4 μm, binned 1 × 1, using the DeltaVision system (Applied Precision) equipped with an IX70 inverted microscope (Olympus), a Plan Apo ×60 objective (1.40 NA), and a CoolSnap HQ digital camera (Photometrics). Exposures were 0.1 s for GFP and 0.15 s for mCherry.

To assay for chromosome biorientation, *CEN3* was visualized using LacI-GFP bound to a LacO-array adjacent to the centromere (Table S1). LacI-GFP is under control of the

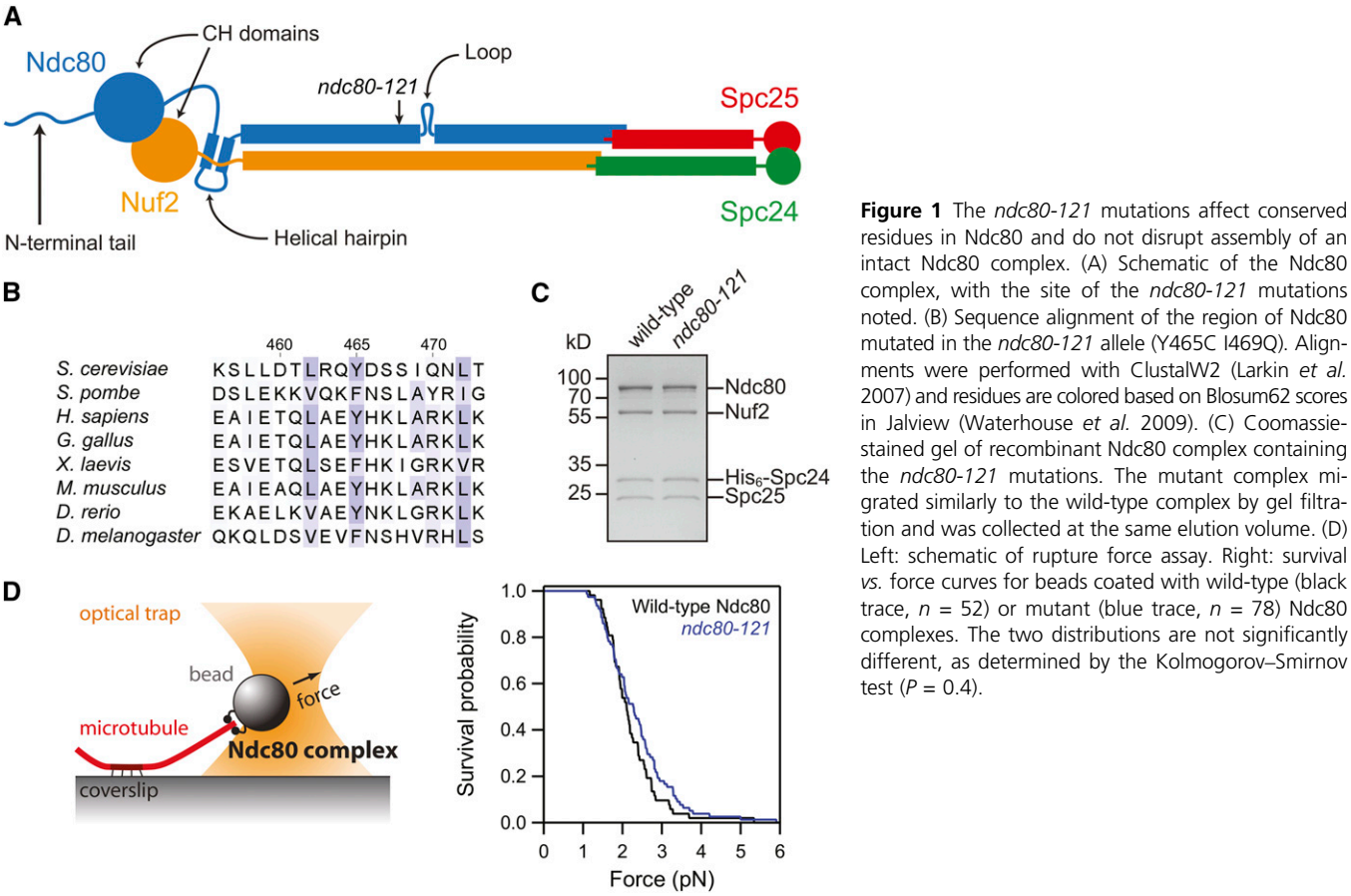

Figure 1 The *ndc80-121* mutations affect conserved residues in Ndc80 and do not disrupt assembly of an intact Ndc80 complex. (A) Schematic of the Ndc80 complex, with the site of the *ndc80-121* mutations noted. (B) Sequence alignment of the region of Ndc80 mutated in the *ndc80-121* allele (Y465C I469Q). Alignments were performed with ClustalW2 (Larkin *et al.* 2007) and residues are colored based on Blosum62 scores in Jalview (Waterhouse *et al.* 2009). (C) Coomassie-stained gel of recombinant Ndc80 complex containing the *ndc80-121* mutations. The mutant complex migrated similarly to the wild-type complex by gel filtration and was collected at the same elution volume. (D) Left: schematic of rupture force assay. Right: survival *vs.* force curves for beads coated with wild-type (black trace, n = 52) or mutant (blue trace, n = 78) Ndc80 complexes. The two distributions are not significantly different, as determined by the Kolmogorov–Smirnov test (P = 0.4).

pCUP1 promoter and imaged using uninduced conditions. For G1 synchronization, *MAT***a** cells were grown to ~60 Klett units at 25° and arrested for 1.5 generations with α-factor. To release from the arrest, cells were collected by filtration, washed with three volumes of YPD, sonicated, and shifted to 37° medium. At 100 min after the release, ~500 μl of cells were harvested by centrifugation and resuspended in media made with yeast nitrogen base without copper (For-Medium). For metaphase arrests, cells with an auxin-inducible Cdc20 degron (Table S1) were first synchronized in G1 with α-factor, then released into media containing 500 μM 3-indoleacetic acid (Sigma-Aldrich) for 1 hr at 25°. The culture was then shifted to 37° for 100 min before harvesting. For imaging, cells were mounted for microscopy as previously described (Muller *et al.* 2005) (instructional video at http://youtu.be/ZrZVbFg9NE8), except that agarose pads were made with yeast nitrogen base without copper (For-Medium). Images were taken with seven z-sections spanning 4.2 μm, binned 1 × 1, using the DeltaVision system (as above) equipped with a U Plan Apo ×100 objective (1.35 NA). Exposures were 0.4 s for GFP and 0.3 s for mCherry.

To image kinetochores, *MAT***a** cells containing Nuf2-GFP and Spc110-mCherry (Table S1) were synchronized in G1 with α-factor (as above) and released into 37° medium for 100 min. After harvesting, cells were mounted on agarose pads (Muller *et al.* 2005) and imaged using the DeltaVision system (as above) equipped with a U Plan Apo ×100 objective (1.35 NA). Images were taken with seven z-sections spanning 4.2 μm, binned 1 × 1. Exposures were 0.4 s for GFP and 0.3 s for mCherry. To determine the kinetochore intensity ratio, the intensities of Nuf2-GFP and Spc110-mCherry were measured (ImageJ). For each spindle, custom programs (available upon request) written in Igor Pro (Wavemetrics) identified the positions of spindle pole bodies based on Gaussian fits to the Spc110-mCherry signal, and calculated the integrated GFP fluorescence intensity on each half of the spindle. The kinetochore intensity ratio is defined as the integrated intensity of the brighter half of the spindle divided by the intensity of the dimmer half (and thus, always ≥1). Box plots of the data were constructed in Igor Pro and statistical analyses were performed using the Kolmogorov–Smirnov test.

In vitro rupture force assay

Recombinant Ndc80 complex was loaded onto 0.44-μm polystyrene beads at a ratio of ~2000 complexes per bead. Bead functionalization was carried out in incubation buffer (BRB80 containing 8 mg·ml^{-1} BSA and 1 mM DTT) for 1 hr at 4° in a total volume of 60 μl. Beads were then pelleted (16,000 × g for 10 min at 4°) and washed with ~200 μl incubation buffer

to remove any unbound Ndc80 complex. Flow chambers were prepared as previously described (Franck *et al.* 2010). Beads were introduced into the flow chamber in assay buffer (BRB80 containing 8 mg·ml^{-1} BSA, 1 mg·ml^{-1} κ-casein, 1 mM DTT, 1 mM GTP, and 1.4 mg·ml^{-1} tubulin) supplemented with an oxygen scavenging system (250 μg·ml^{-1} glucose oxidase, 30 μg·ml^{-1} catalase, and 30 mM glucose). Free tubulin in the assay buffer assembled to form dynamic microtubule extensions from coverslip-anchored Guanosine-5′-[(α,β)-methyleno]triphosphate (GMPCPP)-stabilized microtubule seeds.

A custom optical trap instrument was used to manipulate individual beads in the flow chamber. Rupture force assays were performed as previously described (Franck *et al.* 2010; Tien *et al.* 2010). Each bead was pulled to the end of a dynamic microtubule under a test force of 0.5–1 pN exerted by the trap. Applied force was then increased at a constant rate (0.25 pN·s^{-1}) until the attachment ruptured. The rupture force was indicated by the maximum force attained during each event prior to detachment and determined after the experiment during data analysis from records of force *vs.* time (using custom software, available upon request, written in Igor Pro, Wavemetrics).

Cross-linking of recombinant Ndc80 complex and mass spectrometry analysis

Ndc80 complex (44 μg in 143 μL reaction volume) was cross-linked for 2 min at room temperature with disuccinimidyl suberate (Pierce, 0.3 mM final). The reaction mix was quenched with 10 μl of 500 mM NH_4HCO_3 and the buffer was exchanged to HB500 (40 mM HEPES, 500 mM NaCl, pH 7.5) using protein desalting spin columns (Pierce) according to the manufacturer's protocol. Cross-linked proteins were subsequently reduced with 10 mM dithiothreitol for 30 min at 37°, alkylated with 15 mM iodoacetamide for 30 min at room temperature, and digested with trypsin (at a substrate-to-enzyme ratio of 60:1) overnight at room temperature with shaking. Samples were acidified with 5 M HCl and stored at −80°.

Samples (1.5 μg) were loaded onto a fused-silica capillary tip column (75 μm i.d.) packed with 40 cm of Reprosil-Pur C18-AQ (3-μm bead diameter, Dr. Maisch). Peptides were eluted from the column at 250 nL·min^{-1} using a gradient of 2–35% acetonitrile (in 0.1% formic acid) over 120 min, followed by 35–60% acetonitrile over 10 min. Mass spectrometry was performed on a Q-Exactive (Thermo Scientific), operated using data-dependent acquisition where a maximum of six MS/MS spectra were acquired per MS spectrum (scan range of m/z 400–1600). At m/z 200, the resolution for MS and MS/MS was 70,000 and 35,000, respectively.

Cross-linked peptides were identified using the Kojak cross-link identification software (available at https://code.google.com/p/kojak-ms/). The results of Kojak were exported directly to Percolator (Kall *et al.* 2007) to produce a statistically validated set of cross-linked peptide identifications at a false discovery rate threshold of 5%.

Results

Isolation of the ndc80-121 temperature-sensitive allele

The Ndc80 complex features two globular ends linked by a long, rod-shaped segment composed of predicted coiled-coil domains from all four components (Figure 1A). We recently performed an insertional mutagenesis screen to uncover essential regions of *NDC80* in *S. cerevisiae* (Tien *et al.* 2013). The functions of four of these essential regions, identified as clusters of lethal insertions, have not yet been identified. Insertions from one such cluster located near the disordered loop were found to confer a temperature-sensitive phenotype (Table S2), allowing us to study the function of this loop-proximal region of *NDC80 in vivo*. These temperature-sensitive insertions in *NDC80* mapped to consecutive residues in the protein, disrupting the region from a highly conserved aromatic, Y465, through I469 (Table S2, Figure 1B). We isolated a minimal mutation that was sufficient to recapitulate the temperature-sensitive phenotype: Y465C and I469Q (Figure 1A, Table S2). This allele was named *ndc80-121*.

The ndc80-121 mutations do not affect assembly of the complex or its ability to bind microtubules

We first examined the effects of the *ndc80-121* mutations on the integrity of the mutant Ndc80 complex. When expressed and purified recombinantly, the *ndc80-121* mutations do not disrupt assembly of the heterotetrameric Ndc80 complex (Figure 1C). All four components of the Ndc80 complex were coimmunoprecipitated with Nuf2-TAP from *ndc80-121* yeast cells shifted to the restrictive temperature of 37° (Table S3). These results demonstrate that the temperature-sensitive phenotype of *ndc80-121* cells is not a result of degradation of the Ndc80 complex. Furthermore, the temperature shift to 37° does not lead to disassembly of mutant Ndc80 complexes. We then asked if these mutations disrupt the microtubule attachment strength of the Ndc80 complex, as reported for other temperature-sensitive *ndc80* mutants (*e.g.*, *ndc80-1*; Wigge *et al.* 1998; Pinsky *et al.* 2006; Akiyoshi *et al.* 2010). Using an *in vitro* rupture force assay (Franck *et al.* 2010), we determined that microtubule attachments mediated by wild-type Ndc80 complex ruptured at 2.2 ± 0.1 pN on average (Figure 1D), as previously observed (Tien *et al.* 2010). The attachment strength of the mutant complex was indistinguishable, yielding a mean rupture force of 2.4 ± 0.1 pN (Figure 1D). Therefore, the *ndc80-121* mutations do not affect composition of the Ndc80 complex or its ability to bind microtubules (also see below). Instead, the mutations likely disrupt a specific function of the coiled-coil domain near the loop region.

The ndc80-121 mutations cause a mitotic arrest

The *ndc80-121* allele allows us to interrogate the functions of this uncharacterized region of Ndc80 *in vivo*. To track budding and progression through the cell cycle, we synchronized wild-type and *ndc80-121* cells in G1 and released to

the restrictive temperature. While wild-type cells progressed through mitosis normally (Figure S1A), *ndc80-121* cells accumulated large buds, indicative of a mitotic arrest (Figure S1B). As *ndc80-121* cells entered mitosis, spindle pole bodies (marked by Spc110-mCherry) were able to separate. However, microtubules (visualized by Tub1-GFP) frequently failed to orient along the spindle axis after pole separation (Figure 2A), indicating that *ndc80-121* cells arrest with broken spindles at the restrictive temperature (Figure 2B). This suggests that *ndc80-121* cells might also have a defect in chromosome segregation. To track chromosome biorientation, we utilized a LacO/LacI system to visualize individual centromeres by fluorescence (see *Materials and Methods*). Consistent with an inability to biorient chromosomes, 64% of *ndc80-121* cells did not have separated *CEN3-GFP* spots after 100 min at 37° (compared to 7% of wild-type cells) (Figure 2C).

Using the broken spindle phenotype as a readout, we found that the spindle integrity defect observed in *ndc80-121* cells does not occur if biorientation is first established. We arrested *ndc80-121* cells in metaphase at the permissive temperature using a Cdc20-degron system (Nishimura *et al.* 2009) and subsequently shifted to the restrictive temperature while continuing the metaphase arrest. Similar to wild-type cells, *ndc80-121* cells remained in metaphase; spindles did not break, and chromosome biorientation (visualized by *CEN3-GFP*) was maintained (Figure 2, B and C). Therefore, metaphase kinetochores in *ndc80-121* cells can support microtubule attachments against the tensile forces exerted across bioriented chromosomes. The *ndc80-121* mutations preclude cells from establishing, but not maintaining, a bioriented spindle at the restrictive temperature.

The mitotic defects in ndc80-121 cells are detected by Ipl1

During mitosis, aberrant kinetochore–microtubule attachments are thought to be detected and detached by the conserved Ipl1/Aurora B kinase (Biggins and Murray 2001; Tanaka *et al.* 2002; Pinsky *et al.* 2006). The detachment of kinetochores by Ipl1 causes a "wait" signal to be generated, and anaphase is delayed until proper kinetochore–microtubule attachments are made (Pinsky *et al.* 2006). To determine the basis for mitotic arrest in *ndc80-121* cells, we deleted the checkpoint component *MAD1* and monitored cell cycle progression. These *ndc80-121 mad1*Δ cells bypassed the mitotic arrest seen at the restrictive temperature in *ndc801-121* cells (Figure S1C). Similarly, *ndc80-121 ipl1-321* cells did not arrest in mitosis at the restrictive temperature (Figure S1D). Therefore, the spindle checkpoint is functional in *ndc80-121* cells, and their spindle checkpoint-dependent arrest requires Ipl1.

The dependence of the arrest on Mad1 indicates that *ndc80-121* cells fail to silence the spindle checkpoint wait signal, which is likely generated by unattached kinetochores. To determine if unattached kinetochores persist in *ndc80-121* cells, we visualized kinetochores directly by fluorescence microscopy (with Nuf2-GFP; Figure 3A). During mitosis, kinetochores in wild-type cells are clustered into two distinct spots. By contrast, *ndc80-121* cells have multiple Nuf2-GFP foci located both on and off the spindle axis. Kinetochore declustering off the spindle axis (Figure 3A, arrow) indicates the presence of unattached kinetochores (Anderson *et al.* 2009). At the restrictive temperature, the checkpoint arrest of *ndc80-121* cells also requires Ipl1 (Figure S1D), suggesting that unattached kinetochores are generated in an Ipl1-dependent manner (Pinsky *et al.* 2006). Indeed, kinetochore declustering off the spindle axis was observed 10-fold more frequently in *ndc80-121* cells (18%, $n = 187$ cells) relative to *ndc80-121 ipl1-321* cells (2%, $n = 95$ cells). These results indicate that the *ndc80-121* mutations do not directly lead to detachment of kinetochores from microtubules, but rather cause kinetochores to make erroneous attachments that are subsequently recognized and detached by Ipl1.

To directly assess whether *ndc80-121* cells are defective in kinetochore alignment, we measured their ability to distribute kinetochores equally between the two halves of the spindle. This metric, termed the kinetochore intensity ratio, is obtained by dividing the kinetochore fluorescence intensity of the brighter half of the spindle by the dimmer half (and is thus, by definition, always ≥ 1) (Figure 3, B and C). In wild-type cells, kinetochore distribution was almost perfectly symmetrical, with a median kinetochore intensity ratio of 1.1. Consistent with the requirement of Ipl1 in mitotic error correction, *ip1l-321* cells exhibited a slightly asymmetric kinetochore distribution, with a median ratio of 1.3. *ndc80-121* cells showed a similar kinetochore alignment defect, with a median kinetochore intensity ratio of 1.4. These mutations had a combinatorial effect on kinetochore asymmetry (*ndc80-121 ipl1-321* cells exhibited a median ratio of 1.9), indicating that the activity of Ipl1 mitigates the kinetochore alignment defect in *ndc80-121* cells. Taken together, our results demonstrate that the *ndc80-121* mutations cause the formation of aberrant kinetochore–microtubule attachments that are detached by Ipl1.

Folding of the Ndc80 complex is required for its function in vivo

One possible function of the region in Ndc80 affected by the *ndc80-121* mutations could be the recruitment of an essential binding partner. To identify this putative binding partner, we first performed a screen to isolate dosage-dependent suppressors of the *ndc80-121* mutations. *ndc80-121* cells were transformed with a library containing fragments of the yeast genome cloned into a high-copy vector (Nasmyth and Tatchell 1980) and screened for growth at the restrictive temperature. We screened $\sim 2 \times 10^5$ plasmids (with 5- to 20-kb fragments, resulting in >70 times coverage of the genome) and isolated 41 suppressor fragments, all of which contain the wild-type *NDC80* gene. Results from this screen indicate that overexpression of wild-type *NDC80* can suppress the *ndc80-121* mutations. However, no extragenic suppressors were found.

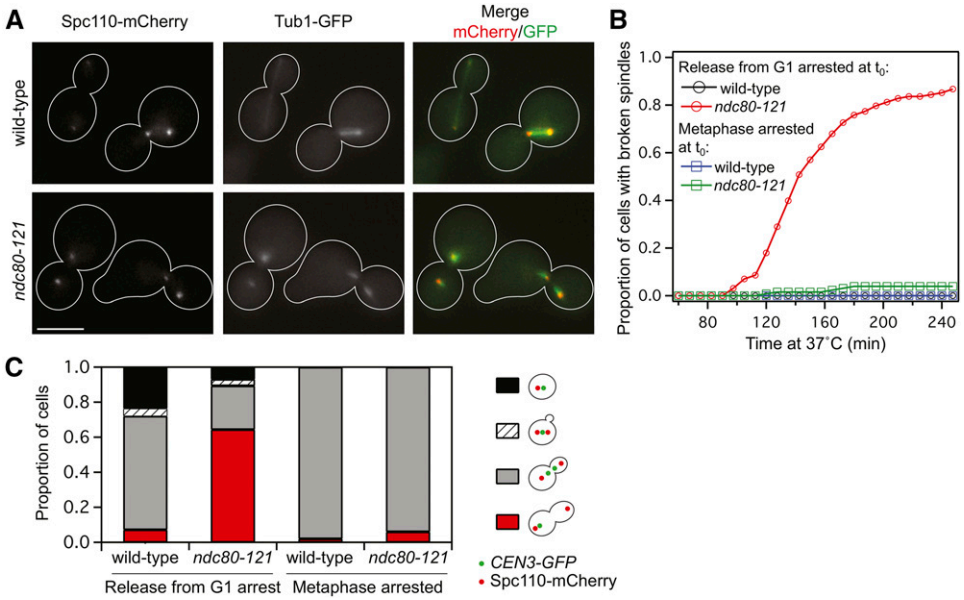

Figure 2 *ndc80-121* cells arrest early in mitosis with broken spindles. (A) Representative images of intact spindles in wild-type cells and broken spindles in *ndc80-121* cells at 37°. Spindle pole bodies were labeled with Spc110-mCherry and microtubules were marked by Tub1-GFP. Bar, 5 μm. (B) Quantification of broken spindles in wild-type and *ndc80-121* cells, which were scored based on microtubule morphology as judged by Tub1-GFP or Stu2-GFP fluorescence. Accumulation of broken spindles was determined after synchronization in G1 and release into 37° medium (n = 119 wild-type cells and n = 128 *ndc80-121* cells), or during a continuous metaphase arrest at 37° (n = 81 wild-type cells and n = 43 *ndc80-121* cells). (C) Biorientation of *CEN3* (visualized using a LacO/LacI-GFP system) in wild-type and *ndc80-121* cells after G1 synchronization and release into 37° medium for 100 min (n = 182 wild-type cells and n = 216 *ndc80-121* cells), or during a continuous metaphase arrest at 37° for 100 min (n = 142 wild-type cells and n = 166 *ndc80-121* cells).

In an independent attempt to identify putative interaction partners, we performed a spontaneous suppressor screen on *ndc80-121* cells to isolate mutations that permit growth at the restrictive temperature. In total, we identified four unique suppressor mutations from screening ~5 × 10^8 *ndc80-121* cells. In *NDC80*, we found one suppressor mutation that restores the wild-type sequence encoding residue 465 (C465Y) (a mutation restoring the wild-type sequence encoding residue 469 (Q469I) was not isolated likely because it requires two base pair substitutions). Additionally, we found two intragenic suppressor mutations in *NDC80*. The first intragenic suppressor mutation, C465F reintroduces an aromatic residue at position 465. The second intragenic suppressor mutation, encoding N564I, is 95 residues downstream of the *ndc80-121* mutations. We named this allele (coding for $Ndc80^{Y465C\ I469Q\ N564I}$) *ndc80-125* (Figure 4). We also generated an allele consisting of the suppressor mutation alone (coding for $Ndc80^{N564I}$), named *ndc80-126*. The *ndc80-126* mutation confers a slow-growth phenotype, which is completely suppressed in the *ndc80-125* allele (the combination of *ndc80-126* and *ndc80-121* mutations, encoding $Ndc80^{Y465C\ I469Q\ N564I}$). Thus, the *ndc80-121* and *ndc80-126* mutations show reciprocal suppression (Figure 4, rows 3, 6, and 10), suggesting that the mutations disrupt the same physical interaction (Honts *et al.* 1994). Lastly, we isolated one extragenic suppressor mutation in *NUF2*, encoding L344S, and named this allele *nuf2-101* (Figure 4). This mutation in Nuf2 is located toward the C terminus of the protein and is predicted to be positioned close to the suppressor mutation $Ndc80^{N564I}$ in the assembled tetrameric complex (see below). The findings from the two suppressor screens suggest that the *ndc80-121* mutations do not directly affect recruitment of another kinetochore component, but rather disrupt an interaction between two parts of the Ndc80 complex.

It was previously proposed from electron microscopy studies that the Ndc80 complex exhibits flexibility *in vitro* by bending about the loop region (Wang *et al.* 2008). The *ndc80-121* mutations and their suppressors lie on opposite sides of the loop. If this genetic interaction reflects a physical interaction, it can be explained by tight folding of the complex at the loop. Therefore, we reasoned that in diploid cells, the intragenic suppressor mutation should only rescue *ndc80-121* in *cis* (*i.e.*, when introduced into the same molecule of Ndc80). Similar to *ndc80-121* haploid cells, *ndc80-121/ndc80-121* homozygous diploid cells are temperature sensitive (Figure 4, row 4). A single copy of the intragenic suppressor mutation introduced in *cis* partially rescues the temperature sensitivity in diploid cells (Figure 4, row 7, *ndc80-125/ndc80-121*; $Ndc80^{Y465C\ I469Q\ N564I}$/$Ndc80^{Y465C\ I469Q}$). However, diploid cells containing the mutant and suppressor mutations on separate alleles are temperature sensitive (Figure 4, row 11, *ndc80-126/ndc80-121*; $Ndc80^{N564I}$/$Ndc80^{Y465C\ I469Q}$). Failure of $Ndc80^{N564I}$ to rescue function of $Ndc80^{Y465C\ I469Q}$ in *trans* suggests that a physical interaction occurs within a single Ndc80 protein (rather than between two or more copies of Ndc80 at the kinetochore). Our characterization of the *ndc80-121* allele and its suppressors suggest that hinging of the Ndc80 complex about its loop is essential for its function *in vivo*.

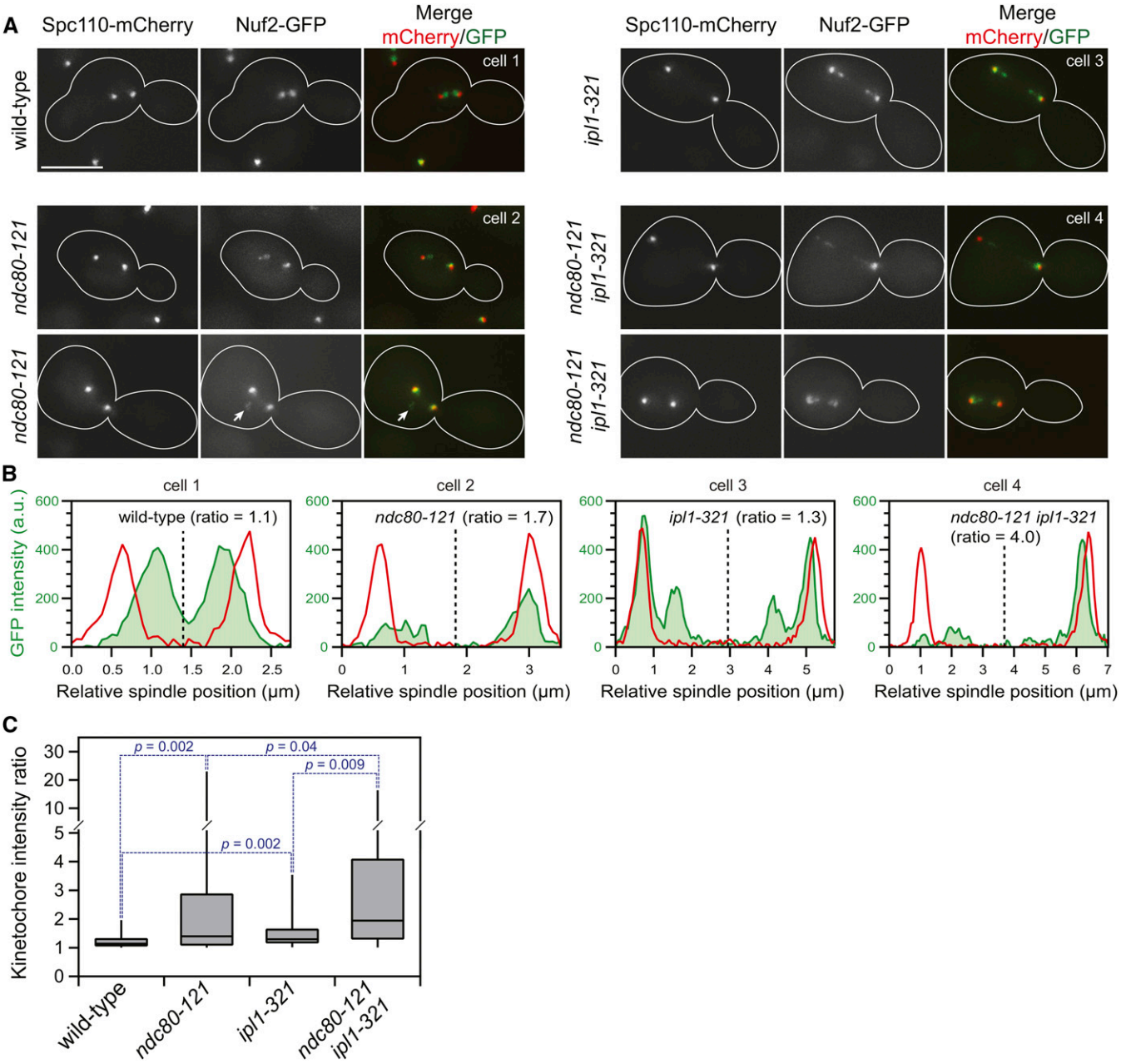

Figure 3 Kinetochores are declustered in *ndc80-121* cells and are targeted by Ipl1. (A) Representative images of kinetochores (Nuf2-GFP) in wild-type, *ndc80-121*, *ipl1-321*, and *ndc80-121 ipl1-321* cells after synchronization in G1 and release into 37° medium for 100 min. Arrow denotes declustered kinetochores off the spindle axis. Bar, 5 μm. (B) From the representative images (cells 1–4), the integrated kinetochore fluorescence (green area) was measured for each half of the spindle, and the kinetochore intensity ratio was calculated. The spindle midline was determined based on the positions of the spindle pole bodies (Spc110-mCherry, red lines). (C) Summary of kinetochore intensity ratios of wild-type and mutant cells (n = 40 cells for each condition). The box and whisker plots denote the 0th, 25th, 50th, 75th, and 100th percentiles of the dataset. Statistical comparisons between the distributions were performed using the Kolmogorov–Smirnov test.

The S. cerevisiae Ndc80 complex can adopt a tightly folded conformation

Additional evidence that the Ndc80 complex adopts a folded conformation came by assessing the structure of recombinant complex *in vitro* by protein cross-linking paired with mass spectrometry analysis. This approach allows the identification of interacting regions within the complex (Figure S2, Table S4, and Table S5). Previously, 26 cross-links were identified within the human Ndc80 complex (Maiolica *et al.* 2007). In addition to providing a higher resolution map of how the Ndc80 complex is organized, cross-linking can also capture transient conformations of the complex. Recombinant *S. cerevisiae* Ndc80 complex was cross-linked with disuccinimidyl suberate, which targets primary amine groups

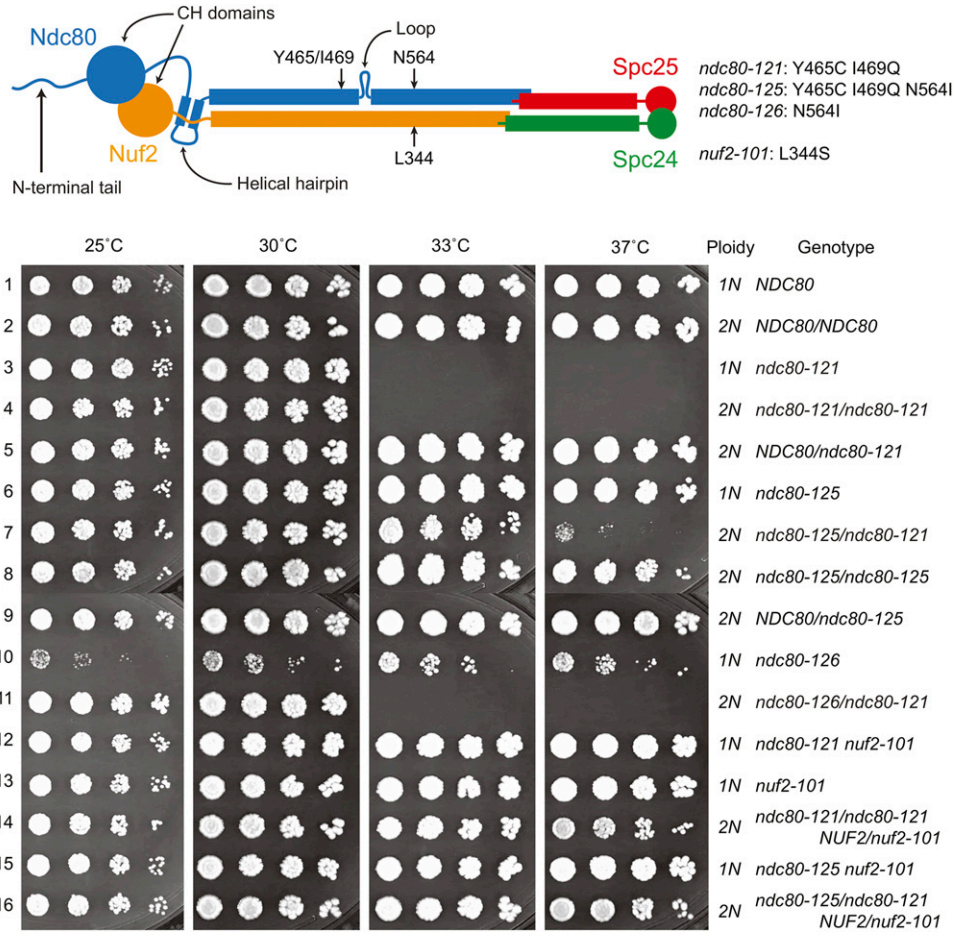

Figure 4 Mutational analyses provide genetic evidence for a folded conformation of the Ndc80 complex *in vivo*. A five-fold dilution series of cells (Table S1) was plated and grown at the indicated temperatures. Two suppressor mutations (encoding N564I in Ndc80 and L344S in Nuf2) can individually rescue growth of *ndc80-121* cells at the restrictive temperature (rows 6 and 12). Mutant alleles encode the following amino acid changes: *ndc80-121* (Y465C I469Q), *ndc80-125* (Y465C I469Q N564I), *ndc80-126* (N564I), and *nuf2-101* (L344S). In a heterozygous diploid, *ndc80-121/ndc80-121* is temperature sensitive (row 4). The N564I intragenic suppressor mutation in Ndc80 can rescue the *ndc80-121* phenotype in *cis*, but not in *trans* (compare rows 7 and 11). The *ndc80-126* allele confers a slow-growth phenotype, which is rescued by the mutations in *ndc80-121* (compare rows 6 and 10).

in lysines and free N termini of proteins. After digestion of the complex with trypsin and mass spectrometric analysis, four different types of peptides (Figure S2A) were identified using Kojak (an open-source application for efficient identification of cross-linked peptides; Hoopmann *et al.* 2014): (i) unlinked peptides, (ii) mono-linked peptides, (iii) loop-linked peptides (cross-link between two amino acids within a single peptide), and (iv) cross-linked peptides (cross-link between two different peptides). Of the 138 lysines in the Ndc80 complex, 128 were identified in mono-links (93%; Figure S2B), suggesting that we have nearly saturated available reactive sites with the cross-linking reagent. Structural information can be determined from the cross-linked peptides, which represent pairs of primary amine groups whose backbone α-carbons are within ~30 Å of one another in the three-dimensional structure of the complex (Herzog *et al.* 2012). In total, our approach revealed 277 unique cross-links and 85 unique loop-links within the Ndc80 complex with ≥95% confidence (Figure S2, C and D, Table S4, and Table S5). The cross-links observed are in excellent agreement with the current structural model of the Ndc80 complex and confirm the location of the tetramerization domain as previously proposed (Wei *et al.* 2005; Maiolica *et al.* 2007; Ciferri *et al.* 2008; Tien *et al.* 2013). The N-terminal tail of Ndc80 cross-linked to multiple regions of the complex (Figure S2, C and D). This is consistent with the extended length of the tail (at least 15 nm, Aravamudhan *et al.* 2014) and its predicted disordered nature (Wei *et al.* 2005, 2007; Ciferri *et al.* 2008; Alushin *et al.* 2010), allowing it to reach multiple parts of the complex in a cross-linking reaction.

Our cross-links establish the register in the coiled coil formed by Ndc80 and Nuf2, revealing two tightly paired segments (Figure 5A, blue and green lines). In each of these regions, the sequences of Ndc80 and Nuf2 maintain a near-constant register, as expected for parallel helices in coiled-coil domains. The region of Ndc80 from K332 to K432 pairs with the Nuf2 region between K169 and K271. Here, the sequences of Ndc80 and Nuf2 are offset by 162 ± 13 residues (n = 23 cross-links; Figure 5A, blue lines). In the second tightly paired segment (Ndc80 from K541 to K632 pairs with Nuf2 from K322 to K409), the offset increases to 216 ± 9 residues (n = 27 cross-links; Figure 5A, green lines). The offset of the two spontaneous suppressor mutations of *ndc80-121* ($Nuf2^{L344S}$ and $Ndc80^{N564I}$) is 220 residues, suggesting they map to directly interacting heptad repeats in the second tightly paired coiled-coil segment. Between the two tightly paired segments, we identified two cross-links that are consistent with a predicted ~50-residue interruption caused by the loop: $Ndc80^{K489}$-$Ndc80^{K513}$ and $Ndc80^{K489}$-$Ndc80^{K522}$ (Figure 5A, orange lines). These cross-links are separated by 24 and 33

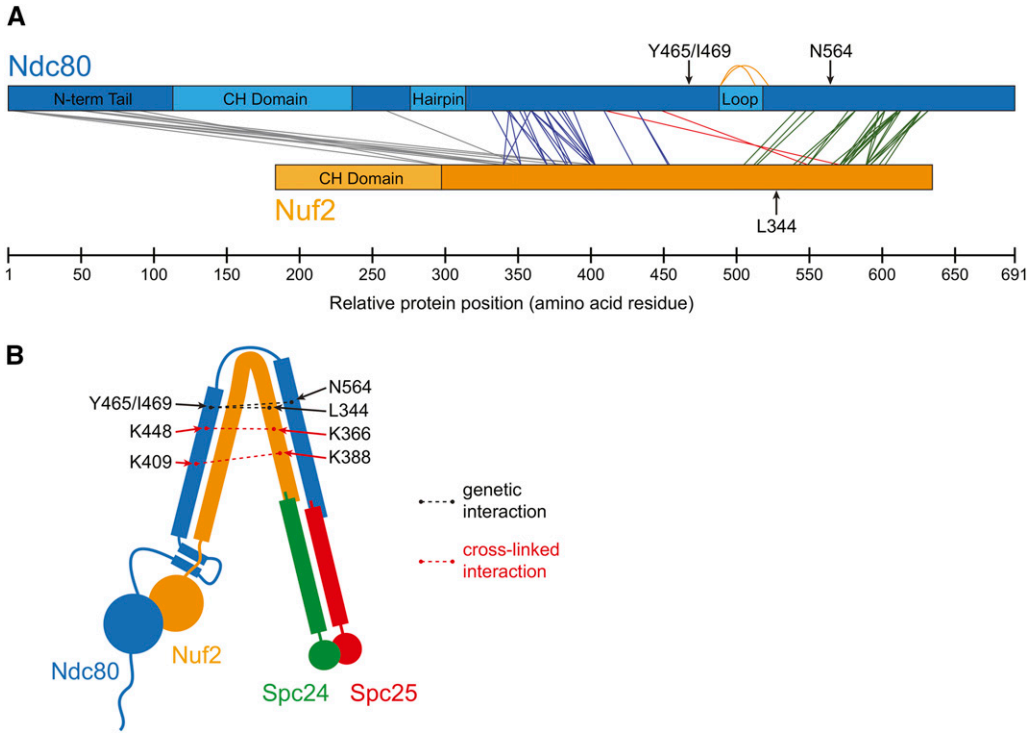

Figure 5 Cross-linking analysis reveals a tightly folded conformation of the Ndc80 complex *in vitro*. (A) From cross-linking analysis of the Ndc80 complex, cross-links between Ndc80 and Nuf2 are shown. Cross-links showing the register between Ndc80 and Nuf2 coiled coils are presented as blue and green lines. Orange lines denote loop-links that support the presence of a loop predicted in the coiled-coil region of Ndc80. Cross-links consistent with a tightly folded conformation of the Ndc80 complex are shown as red lines. Full cross-linking results are diagrammed in Figure S2 and listed in Table S4 and Table S5. (B) A tightly folded conformation of the Ndc80 complex can explain the observed genetic and cross-linked interactions.

residues, respectively. Our cross-linker is too short to span a continuous α-helical segment of even 24 residues in a coiled coil (~1.47-Å rise per residue; discussed in Lupas and Gruber 2005). Instead, these cross-links indicate that the two predicted ends of the loop lie close together. Our cross-links are consistent with and extend the previous results obtained with the human Ndc80 complex and suggest that the coiled coils and interrupting loop are conserved structural features (Maiolica *et al.* 2007).

We found two cross-links that contradict the clear coiled-coil registrations between Ndc80 and Nuf2 (Figure 5A, red lines). These cross-links ($Ndc80^{K409}$-$Nuf2^{K388}$ and $Ndc80^{K448}$-$Nuf2^{K366}$), which were identified with high confidence ($q = 0.01$) and manually validated, connect regions of the complex separated by >130 residues in Ndc80 (Figure 5A). They can be explained if the Ndc80 complex forms a tightly folded conformation by hinging about its loop to bring the two coiled-coil segments in close proximity (Figure 5B). Folding of the complex, as predicted by the cross-links, also brings the suppressor mutations in close proximity to the temperature-sensitive *ndc80-121* mutations. Our characterization of the *ndc80-121* mutant suggests that this conformational change in the complex is required for kinetochore alignment and biorientation during mitosis.

Discussion

The Ndc80 complex folds in half at a flexible loop in Ndc80 early in mitosis

The Ndc80 protein is hypothesized to contain a flexible loop, based on a break in the predicted coiled-coil character (Figure S3). It was previously proposed that the loop acts as a hinge, conferring the flexibility observed for recombinant Ndc80 complexes on negative-stain electron micrographs (Wang *et al.* 2008). Super-resolution microscopy experiments further suggested that different conformations of the Ndc80 complex exist *in vivo*; the distance between the two ends of the Ndc80 complex decreases from ~40 nm to ~20 nm during the metaphase-to-anaphase transition in *S. cerevisiae* (Aravamudhan *et al.* 2014). Altogether, these results predict that the Ndc80 complex undergoes a conformational change through bending at the loop region. Here, we provide two independent lines of evidence that support and extend this model and further show that folding of the complex is of physiological importance. First, we identified cross-links that are consistent with a tightly folded conformation of the Ndc80 complex, bending at the loop region (Figure 5B, dotted red lines). A previous study with the human Ndc80 complex also observed one cross-link that bridges two distant regions of the complex (Maiolica *et al.* 2007). Second, the *ndc80-121* mutant allele and its suppressor mutations demonstrate a genetic interaction between two parts of Ndc80 that can be explained by a folded conformation of the complex (Figure 5B, dotted black lines). We favor a model in which the *ndc80-121* temperature-sensitive phenotype results from a weaker interaction between $Ndc80^{Y465/I469}$ (*ndc80-121* mutation sites) and $Ndc80^{N564}$/$Nuf2^{L344}$ (spontaneous suppressor mutation sites). Furthermore, our observation that the intragenic $Ndc80^{N564I}$ suppressor mutation can only rescue the *ndc80-121* phenotype in *cis* suggests that this physical interaction occurs within a single complex.

Several observations support our hypothesis that the *ndc80-121* mutations destabilize a physical interaction that underlies the tightly folded conformation of the Ndc80 complex. First, the reciprocal suppression between the *ndc80-121* and *ndc80-126* alleles suggests that the corresponding

mutations affect a physical interaction between the two halves of a folded Ndc80 complex (Honts *et al.* 1994). Second, the *ndc80-121* mutant is temperature sensitive, suggesting that both higher temperature and the *ndc80-121* mutations decrease the stability of the folded conformation. By contrast, the suppressor mutation *ndc80-126* confers slow growth at all temperatures, suggesting that this mutation hyperstabilizes the folded conformation, which functions poorly at all growth temperatures. When the *ndc80-121* and *ndc80-126* mutations are combined in *cis* (*i.e.*, the *ndc80-125* allele), their opposing effects on the stability of the folded conformation balance out and restore normal Ndc80 function. Finally, the *ndc80-121* mutant displays no defects when shifted to the restrictive temperature in metaphase, when the Ndc80 complex has been shown to be in an extended conformation (Joglekar *et al.* 2009; Aravamudhan *et al.* 2014). We propose that the mutant complex prematurely adopts a "metaphase-like" extended conformation prior to biorientation, and that the phenotype of *ndc80-121* cells results from an inability to stabilize a closed conformation early in mitosis.

ndc80-121 cells are defective in the resolution of aberrant kinetochore–microtubule attachments

When shifted to the restrictive temperature prior to entry into mitosis, the *ndc80-121* mutant arrests in mitosis with defects in chromosome biorientation. We show that *ndc80-121* cells contain aberrant kinetochore–microtubule attachments that are detached in an Ipl1-dependent manner. It is generally accepted that Ipl1 selectively detaches kinetochores that experience low levels of tension, which can include kinetochores that form either syntelic or weak microtubule attachments (Nicklas and Koch 1969; Biggins and Murray 2001; Tanaka *et al.* 2002; Liu *et al.* 2009; Cane *et al.* 2013). We find that the *ndc80-121* mutations do not weaken the microtubule attachment strength of the Ndc80 complex *in vitro* and that metaphase kinetochores in *ndc80-121* cells can support tension across bioriented chromosomes at the restrictive temperature *in vivo*. Furthermore, *ndc80-121 ipl1-321* cells are not arrested by the spindle checkpoint, indicating that the *ndc80-121* mutations do not by themselves produce a major attachment defect without the detachment-promoting activity of Ipl1. Based on these observations, we favor a model where the Ipl1-dependent arrest of *ndc80-121* cells is due to the presence of syntelic attachments (that are targeted for detachment by Ipl1), which are not fully resolved before spindle breakage. Consistent with a higher prevalence of syntelic attachments, kinetochores in *ndc80-121* cells are asymmetrically distributed on the spindle, similar to those in *ipl1-321* cells. This kinetochore alignment defect is further exacerbated in the *ndc80-121 ipl1-321* double mutant. This observation rules out the possibility that kinetochore–microtubule attachments in *ndc80-121* cells are correct, but anomalously targeted by Ipl1. The more severe kinetochore alignment defect in *ndc80-121 ipl1-321* as compared to *ipl1-321* cells further suggests that *ndc80-121* kinetochores have a greater tendency to form incorrect attachments than wild-type kinetochores (Figure 6). This could result from changes in the conformation of the Ndc80 complex that favor syntelic attachment geometry. In an alternative, but not mutually exclusive model, aberrant attachments in *ndc80-121* cells are not efficiently detached in response to Ipl1 activity (Figure 6). In both scenarios, the persistence of erroneous attachments in *ndc80-121* cells overwhelms the Ipl1-dependent error correction machinery, resulting in spindle breakage.

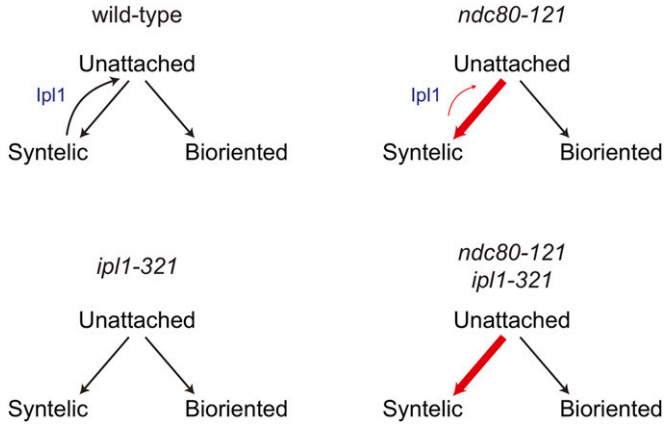

Figure 6 A model for how *ndc80-121* cells generate kinetochore alignment defects. The *ndc80-121* allele causes more stable syntelic attachments, which are not effectively resolved by Ipl1 kinase.

The structural architecture of the Ndc80 complex, including its inherent flexibility, is highly conserved (Maiolica *et al.* 2007; Wang *et al.* 2008). Furthermore, the *ndc80-121* mutations affect conserved residues in Ndc80 (Figure 1B), suggesting that a physical interaction stabilizes a folded conformation of the Ndc80 complex in higher eukaryotes. Together, our results suggest that folding of Ndc80 complex and its role in the resolution of aberrant kinetochore–microtubule attachments are common features in eukaryotic cells.

Acknowledgments

We thank Rachel Klevit, Michelle Giarmarco, Justin Decarreau, and Linda Wordeman for advice and technical assistance. We also thank members of the Davis lab and the Seattle Mitosis group for helpful discussions and Matthew Miller for critical reading of this manuscript. This work was supported by a National Sciences and Engineering Research Council of Canada scholarship to J.F.T.; National Institutes of Health grant no. T32 GM008268 to N.T.U.; National Center for Research Resources grant no. S10 RR26406 to C.L.A.; and National Institute of General Medical Sciences grant nos. R01 GM040506 to T.N.D. and R01 GM079373 to C.L.A. This work was also supported in part by the National Science Foundation MRI grant no. 0923536, and the National Institute of General Medical Sciences under grant nos. 2P50 GM076547/Center for Systems Biology, and GM087221, and grant no. S10RR027584 to R.L.M. M.R., M.J.M., B.R.F. and J.R.Y. were supported by grant no. P41 GM103533 to T.N.D.

Literature Cited

Akiyoshi, B., K. K. Sarangapani, A. F. Powers, C. R. Nelson, S. L. Reichow *et al.*, 2010 Tension directly stabilizes reconstituted kinetochore-microtubule attachments. Nature 468: 576–579.

Alushin, G. M., V. H. Ramey, S. Pasqualato, D. A. Ball, N. Grigorieff *et al.*, 2010 The Ndc80 kinetochore complex forms oligomeric arrays along microtubules. Nature 467: 805–810.

Anderson, M., J. Haase, E. Yeh, and K. Bloom, 2009 Function and assembly of DNA looping, clustering, and microtubule attachment complexes within a eukaryotic kinetochore. Mol. Biol. Cell 20: 4131–4139.

Aravamudhan, P., I. Felzer-Kim, K. Gurunathan, and A. P. Joglekar, 2014 Assembling the protein architecture of the budding yeast kinetochore-microtubule attachment using FRET. Curr. Biol. 24: 1437–1446.

Biggins, S., and A. W. Murray, 2001 The budding yeast protein kinase Ipl1/Aurora allows the absence of tension to activate the spindle checkpoint. Genes Dev. 15: 3118–3129.

Biggins, S., N. Bhalla, A. Chang, D. L. Smith, and A. W. Murray, 2001 Genes involved in sister chromatid separation and segregation in the budding yeast Saccharomyces cerevisiae. Genetics 159: 453–470.

Cane, S., A. A. Ye, S. J. Luks-Morgan, and T. J. Maresca, 2013 Elevated polar ejection forces stabilize kinetochore-microtubule attachments. J. Cell Biol. 200: 203–218.

Ciferri, C., S. Pasqualato, E. Screpanti, G. Varetti, S. Santaguida *et al.*, 2008 Implications for kinetochore-microtubule attachment from the structure of an engineered Ndc80 complex. Cell 133: 427–439.

De Wulf, P., A. D. McAinsh, and P. K. Sorger, 2003 Hierarchical assembly of the budding yeast kinetochore from multiple subcomplexes. Genes Dev. 17: 2902–2921.

Franck, A. D., A. F. Powers, D. R. Gestaut, T. N. Davis, and C. L. Asbury, 2010 Direct physical study of kinetochore-microtubule interactions by reconstitution and interrogation with an optical force clamp. Methods 51: 242–250.

Hauf, S., 2013 The spindle assembly checkpoint: progress and persistent puzzles. Biochem. Soc. Trans. 41: 1755–1760.

Herzog, F., A. Kahraman, D. Boehringer, R. Mak, A. Bracher *et al.*, 2012 Structural probing of a protein phosphatase 2A network by chemical cross-linking and mass spectrometry. Science 337: 1348–1352.

Honts, J. E., T. S. Sandrock, S. M. Brower, J. L. O'Dell, and A. E. Adams, 1994 Actin mutations that show suppression with fimbrin mutations identify a likely fimbrin-binding site on actin. J. Cell Biol. 126: 413–422.

Janke, C., J. Ortiz, J. Lechner, A. Shevchenko, M. M. Magiera *et al.*, 2001 The budding yeast proteins Spc24p and Spc25p interact with Ndc80p and Nuf2p at the kinetochore and are important for kinetochore clustering and checkpoint control. EMBO J. 20: 777–791.

Joglekar, A. P., K. Bloom, and E. D. Salmon, 2009 In vivo protein architecture of the eukaryotic kinetochore with nanometer scale accuracy. Curr. Biol. 19: 694–699.

Kall, L., J. D. Canterbury, J. Weston, W. S. Noble, and M. J. MacCoss, 2007 Semi-supervised learning for peptide identification from shotgun proteomics datasets. Nat. Methods 4: 923–925.

Larkin, M. A., G. Blackshields, N. P. Brown, R. Chenna, P. A. McGettigan *et al.*, 2007 Clustal W and Clustal X version 2.0. Bioinformatics 23: 2947–2948.

Liu, D., G. Vader, M. J. Vromans, M. A. Lampson, and S. M. Lens, 2009 Sensing chromosome bi-orientation by spatial separation of aurora B kinase from kinetochore substrates. Science 323: 1350–1353.

Lupas, A. N., and M. Gruber, 2005 The structure of alpha-helical coiled coils. Adv. Protein Chem. 70: 37–78.

Maiolica, A., D. Cittaro, D. Borsotti, L. Sennels, C. Ciferri *et al.*, 2007 Structural analysis of multiprotein complexes by cross-linking, mass spectrometry, and database searching. Mol. Cell. Proteomics 6: 2200–2211.

Malvezzi, F., G. Litos, A. Schleiffer, A. Heuck, K. Mechtler *et al.*, 2013 A structural basis for kinetochore recruitment of the Ndc80 complex via two distinct centromere receptors. EMBO J. 32: 409–423.

Muller, E. G. D., B. E. Snydsman, I. Novik, D. W. Hailey, D. R. Gestaut *et al.*, 2005 The organization of the core proteins of the yeast spindle pole body. Mol. Biol. Cell 16: 3341–3352.

Nasmyth, K. A., and K. Tatchell, 1980 The structure of transposable yeast mating type loci. Cell 19: 753–764.

Nicklas, R. B., and C. A. Koch, 1969 Chromosome micromanipulation. 3. Spindle fiber tension and the reorientation of mal-oriented chromosomes. J. Cell Biol. 43: 40–50.

Nishimura, K., T. Fukagawa, H. Takisawa, T. Kakimoto, and M. Kanemaki, 2009 An auxin-based degron system for the rapid depletion of proteins in nonplant cells. Nat. Methods 6: 917–922.

Nishino, T., F. Rago, T. Hori, K. Tomii, I. M. Cheeseman *et al.*, 2013 CENP-T provides a structural platform for outer kinetochore assembly. EMBO J. 32: 424–436.

Osborne, M. A., G. Schlenstedt, T. Jinks, and P. A. Silver, 1994 Nuf2, a spindle pole body-associated protein required for nuclear division in yeast. J. Cell Biol. 125: 853–866.

Pinsky, B. A., C. Kung, K. M. Shokat, and S. Biggins, 2006 The Ipl1-Aurora protein kinase activates the spindle checkpoint by creating unattached kinetochores. Nat. Cell Biol. 8: 78–83.

Powers, A. F., A. D. Franck, D. R. Gestaut, J. Cooper, B. Gracyzk *et al.*, 2009 The Ndc80 kinetochore complex forms load-bearing attachments to dynamic microtubule tips via biased diffusion. Cell 136: 865–875.

Tanaka, T. U., N. Rachidi, C. Janke, G. Pereira, M. Galova *et al.*, 2002 Evidence that the Ipl1-Sli15 (Aurora kinase-INCENP) complex promotes chromosome bi-orientation by altering kinetochore-spindle pole connections. Cell 108: 317–329.

Tien, J. F., N. T. Umbreit, D. R. Gestaut, A. D. Franck, J. Cooper *et al.*, 2010 Cooperation of the Dam1 and Ndc80 kinetochore complexes enhances microtubule coupling and is regulated by aurora B. J. Cell Biol. 189: 713–723.

Tien, J. F., K. K. Fong, N. T. Umbreit, C. Payen, A. Zelter *et al.*, 2013 Coupling unbiased mutagenesis to high-throughput DNA sequencing uncovers functional domains in the Ndc80 kinetochore protein of Saccharomyces cerevisiae. Genetics 195: 159–170.

Wang, H. W., S. Long, C. Ciferri, S. Westermann, D. Drubin *et al.*, 2008 Architecture and flexibility of the yeast Ndc80 kinetochore complex. J. Mol. Biol. 383: 894–903.

Waterhouse, A. M., J. B. Procter, D. M. Martin, M. Clamp, and G. J. Barton, 2009 Jalview Version 2–a multiple sequence alignment editor and analysis workbench. Bioinformatics 25: 1189–1191.

Wei, R. R., P. K. Sorger, and S. C. Harrison, 2005 Molecular organization of the Ndc80 complex, an essential kinetochore component. Proc. Natl. Acad. Sci. USA 102: 5363–5367.

Wei, R. R., J. Al-Bassam, and S. C. Harrison, 2007 The Ndc80/HEC1 complex is a contact point for kinetochore-microtubule attachment. Nat. Struct. Mol. Biol. 14: 54–59.

Wigge, P. A., and J. V. Kilmartin, 2001 The Ndc80p complex from Saccharomyces cerevisiae contains conserved centromere components and has a function in chromosome segregation. J. Cell Biol. 152: 349–360.

Wigge, P. A., O. N. Jensen, S. Holmes, S. Soues, M. Mann *et al.*, 1998 Analysis of the Saccharomyces spindle pole by matrix-assisted laser desorption/ionization (MALDI) mass spectrometry. J. Cell Biol. 141: 967–977.

Communicating editor: O. Cohen-Fix

GENETICS

Supporting Information
http://www.genetics.org/lookup/suppl/doi:10.1534/genetics.114.167775/-/DC1

Kinetochore Biorientation in *Saccharomyces cerevisiae* Requires a Tightly Folded Conformation of the Ndc80 Complex

Jerry F. Tien, Neil T. Umbreit, Alex Zelter, Michael Riffle, Michael R. Hoopmann, Richard S. Johnson, Bryan R. Fonslow, John R. Yates, III, Michael J. MacCoss, Robert L. Moritz, Charles L. Asbury, and Trisha N. Davis

DOI: 10.1534/genetics.114.167775

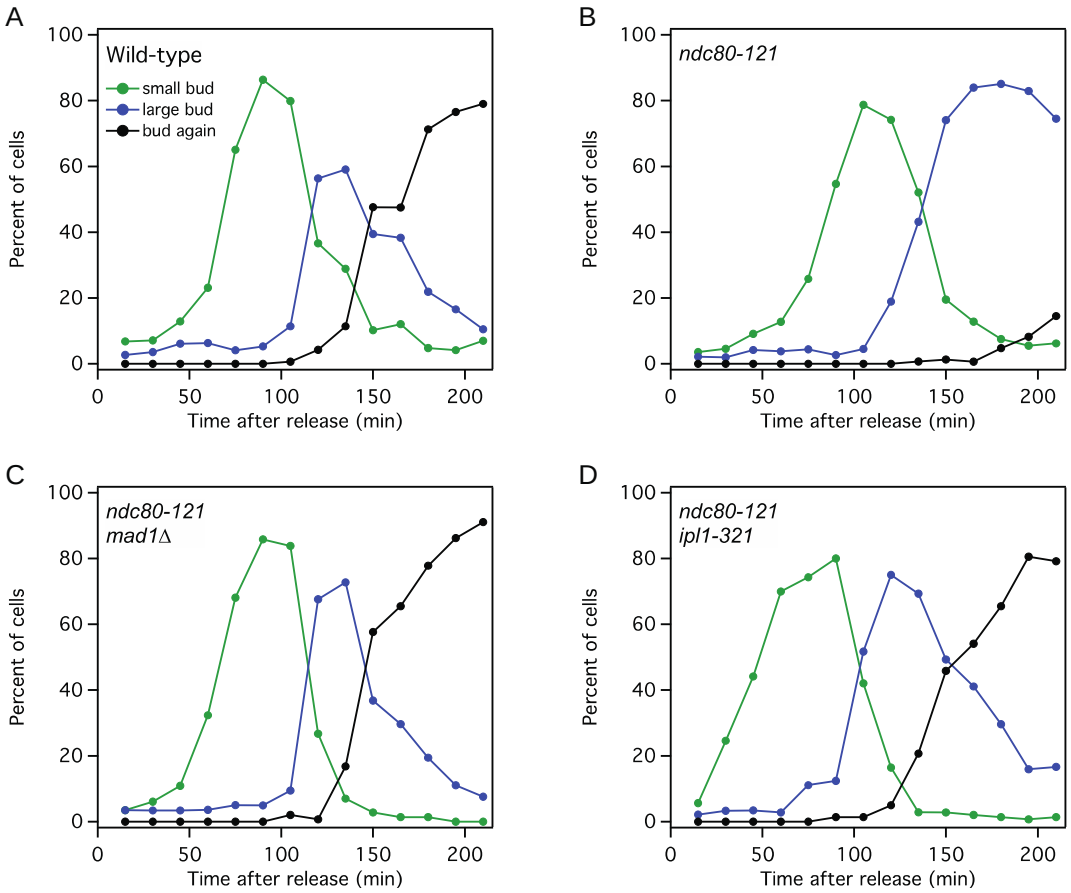

Figure S1 The mitotic arrest of *ndc80-121* cells is dependent on Ipl1 activity and the spindle checkpoint. Budding indices for (A) wild-type, (B) *ndc80-121*, (C) *ipl1-321*, and (D) *ndc80-121 ipl1-321* cells after synchronization at G1 and release into 37˚C medium. At 37˚C, large-budded *ndc80-121* cells exhibit broken spindles and fail to undergo anaphase (Figure 2A and B).

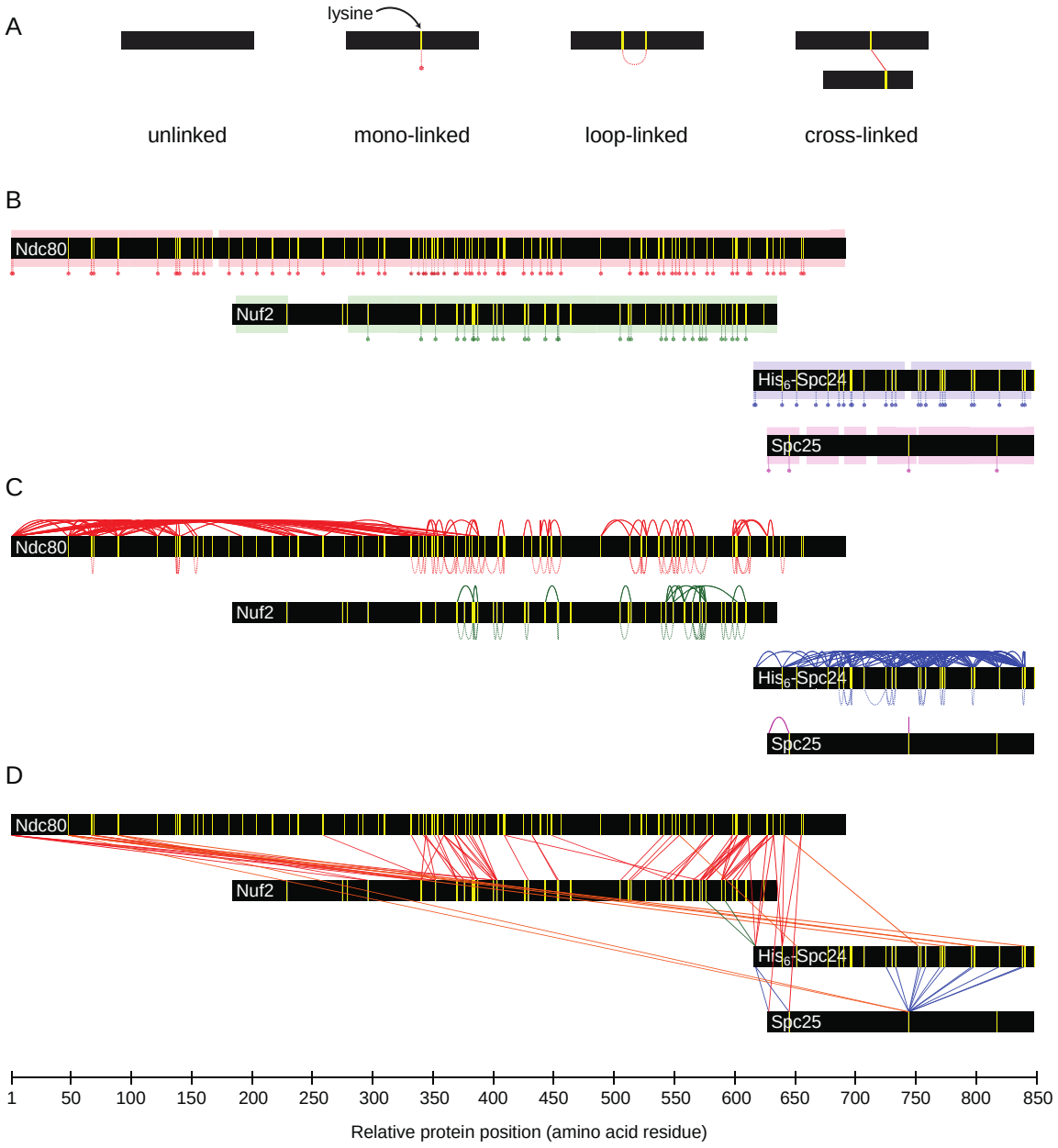

Figure S2 Summary of cross-linking study on wild-type recombinant *S. cerevisiae* Ndc80 complex. (A) After cross-linking and trypsin digestion, four possible peptides were identified by mass spectrometry. (B-D) Diagram representation of cross-linking results for Ndc80, Nuf2, His_6-Spc24, and Spc25 (black bars). (B) Peptide sequence coverage (colored boxes) and mono-links (dotted vertical lines and circles). (C) Loop-links (dotted lines) and self cross-links (solid lines, cross-links between two peptides from the same protein). (D) Cross-links between different proteins (solid line). Vertical yellow lines denote positions of lysines. Full lists of cross-linking results are shown in Tables S4 and S5.

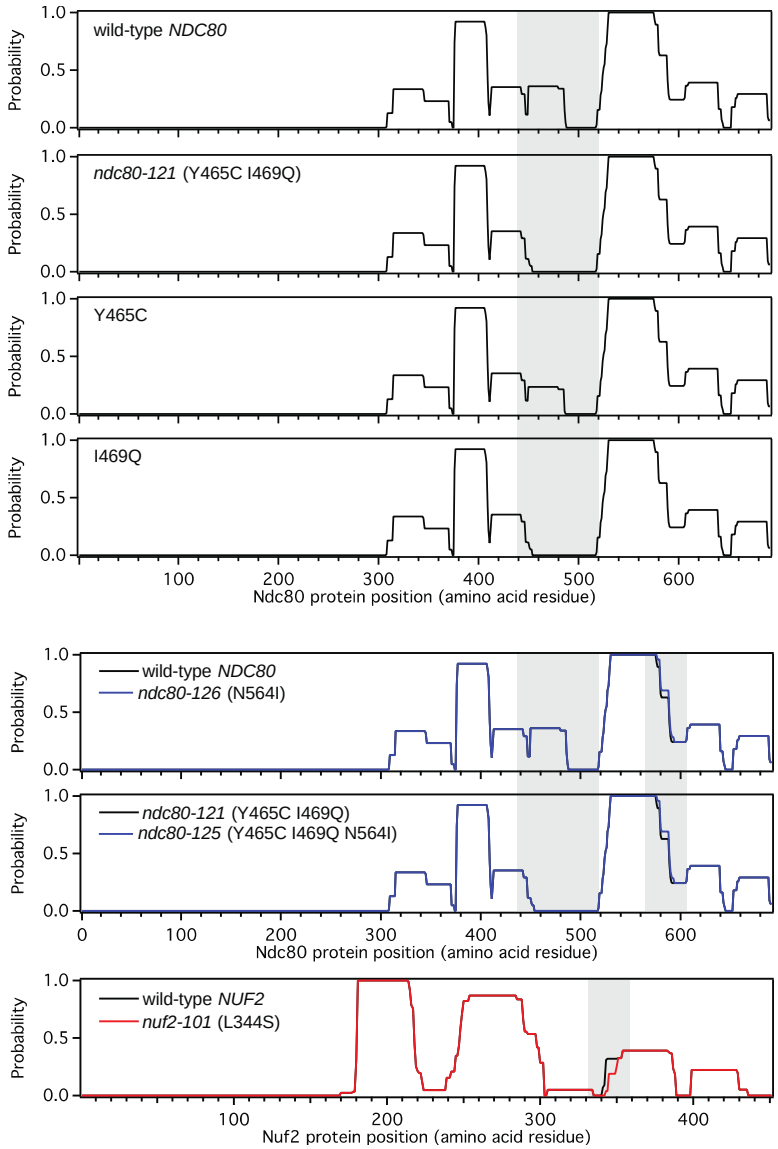

Figure S3 The effects of mutations in Ndc80 and Nuf2 on predicted coiled-coil formation. The probabilities of coiled-coil formation, as predicted by Paircoil2 (McDonnell *et al.* 2006), for Ndc80 or Nuf2 containing the indicated mutations. Where genotypes are shown (in italics), the mutations in the translated protein sequences are shown in brackets. Areas of interest are highlighted in grey boxes.

Table S1 Yeast strains used in this study[a]

Strain	Genotype	Reference
W303	*ade2-1oc can1-100 his3-11,15 leu2-3,112 trp1-1 ura3-1*	
CRY1	MAT**a**	GEISER *et al.* (1993)
JTY14	MAT**a** *ade3Δ-100 lys2Δ::HIS3 ndc80(Y465C)*	This study
JTY23	MAT**a** *ade3Δ-100 lys2Δ::HIS3 ndc80(I469Q)*	This study
JTY8	MAT**a** *ade3Δ-100 lys2Δ::HIS3 ndc80-121*	This study
JTY13	MAT**a** *ade3Δ-100 lys2Δ::HIS3 ndc80(S467A S468A)*	This study
JTY17	MAT**a** *ade3Δ-100 lys2Δ::HIS3 ndc80(S467D S468D)*	This study
JTY18	MAT**a** *ade3Δ-100 lys2Δ::HIS3 ndc80(D466G)*	This study
JTY30-4A	MAT**a** *ade3Δ-100 NUF2-TAP::KanMX NDC80*	This study
JTY30-1A	MAT**a** *ade3Δ-100 NUF2-TAP::KanMX ndc80-121*	This study
JTY58-2D	MAT**a** *ade3Δ-100 lys2Δ::HIS3 SPC110-mCherry::hphMX NDC80*	This study
JTY59-8D	MAT**a** *ade3Δ-100 cyh2^r lys2Δ::HIS3 SPC110-mCherry::hphMX ndc80-121*	This study
JTY96-14C	MAT**a** *ade3Δ-100 lys2Δ::HIS3 SPC110-mCherry::hphMX ndc80-121 mad1Δ::URA3*	This study
JTY98-4B	MAT**a** *ade3Δ-100 SPC110-mCherry::hphMX ndc80-121 ipl1-321*	This study
JTY9-4A	MAT**a** *ade3Δ-100 URA3::TUB1-GFP SPC110-mCherry::hphMX NDC80*	This study
JTY9-10D	MAT**a** *ade3Δ-100 lys2Δ::HIS3 URA3::TUB1-GFP SPC110-mCherry::hphMX ndc80-121*	This study
JTY59-12D	MAT**a** *ade3Δ-100 lys2Δ::HIS3 STU2-GFP::NatMX SPC110-mCherry::hphMX NDC80*	This study
JTY59-7A	MAT**a** *ade3Δ-100 lys2Δ::HIS3 STU2-GFP::NatMX SPC110-mCherry::hphMX ndc80-121*	This study
JTY73-17C	MAT**a** *ade3Δ-100 lys2Δ::HIS3 STU2-GFP::NatMX SPC110-mCherry::hphMX CDC20-AID::KanMX ura3::pADH1-OsTIR1-9myc::URA3 NDC80*	This study
JTY73-2A	MATα *ADE3 STU2-GFP::NatMX SPC110-mCherry::hphMX CDC20-AID::KanMX ura3::pADH1-OsTIR1-9myc::URA3 ndc80-121*	This study
MMWY61#2	MAT**a** *ade3Δ-100 pCUP1-GFP12LacI12::HIS3 CEN3-LacO33array::KanMX SPC110-mCherry::hphMX NDC80*	WARGACKI *et al.* (2010)
JTY65-16B	MAT**a** *ade3Δ-100 pCUP1-GFP12LacI12::HIS3 CEN3-LacO33array::KanMX SPC110-mCherry::hphMX ndc80-121*	This study
JTY112-58A	MAT**a** *ade3Δ-100 lys2Δ::HIS3 pCUP1-GFP12-LacI12::HIS3 CEN3::33LacO::KanMX SPC110-mCherry::hphMX CDC20-AID::KanMX ura3::pADH1-OsTIR1-9myc::URA3 NDC80*	This study
JTY112-20B	MAT**a** *ADE3 lys2Δ::HIS3 pCUP1-GFP12-LacI12::HIS3 CEN3::33LacO::KanMX SPC110-mCherry::hphMX CDC20-AID::KanMX ura3::pADH1-OsTIR1-9myc::URA3 ndc80-121*	This study
JTY11-5A	MAT**a** *ade3Δ-100 NUF2-GFP::HIS3 SPC110-mCherry::hphMX NDC80*	This study
JTY11-16A	MAT**a** *ade3Δ-100 NUF2-GFP::HIS3 SPC110-mCherry::hphMX ndc80-121*	This study
MSY284-8D	MAT**a** *ade3Δ-100 NUF2-GFP::HIS3 SPC110-mCherry::hphMX ipl1-321*	Michelle M. Shimogawa
JTY98-13D	MAT**a** *ade3Δ-100 NUF2-GFP::HIS3 SPC110-mCherry::hphMX ndc80-121 ipl1-321*	This study
KGY315	MAT**a**/MATα *ADE3/ade3Δ-100 cyh2^r/CYH2^s*	GREENLAND *et al.* (2010)
JTY82	MAT**a**/MATα *ade3Δ-100/ade3Δ-100 cyh2^r/cyh2^r lys2Δ::HIS3/lys2Δ::HIS3 ndc80-121/ndc80-121*	This study
JTY74	MAT**a**/MATα *ade3Δ-100/ADE3 cyh2^r/CYH2^s lys2Δ::HIS3/LYS2 ndc80-121/NDC80*	This study
JTY83	MAT**a** *ade3Δ-100 lys2Δ::HIS3 ndc80-125*	This study
JTY81	MAT**a**/MATα *ade3Δ-100/ade3Δ-100 cyh2^r/cyh2^r lys2Δ::HIS3/lys2Δ::HIS3 ndc80-121/ndc80-125*	This study

Strain	Genotype	Reference
JTY102	MAT**a**/MATα *ade3Δ-100/ade3Δ-100 cyh2^r/cyh2^r lys2Δ::HIS3/lys2Δ::HIS3 ndc80-125/ndc80-125*	This study
JTY79	MAT**a**/MATα *ade3Δ-100/ADE3 cyh2^r/CYH2^s lys2Δ::HIS3/LYS2 ndc80-125/NDC80*	This study
JTY114	MAT**a** *ade3Δ-100 cyh2^r lys2Δ::HIS3 ndc80-126*	This study
JTY116	MAT**a**/MATα *ade3Δ-100/ade3Δ-100 cyh2^r/cyh2^r lys2Δ::HIS3/lys2Δ::HIS3 ndc80-126/ndc80-121*	This study
JTY84	MAT**a** *ade3Δ-100 lys2Δ::HIS3 ndc80-121 nuf2-101*	This study
JTY86-5C	MAT**a** *ade3Δ-100 cyh2^r lys2Δ::HIS3 NDC80 nuf2-101*	This study
JTY88	MAT**a**/MATα *ade3Δ-100/ade3Δ-100 cyh2^r/cyh2^r lys2Δ::HIS3/lys2Δ::HIS3 ndc80-121/ndc80-121 nuf2-101/NUF2*	This study
JTY101-6B	MAT**a** *ade3Δ-100 cyh2^r lys2Δ::HIS3 ndc80-125 nuf2-101*	This study
JTY101	MAT**a**/MATα *ade3Δ-100/ade3Δ-100 cyh2^r/cyh2^r lys2Δ::HIS3/lys2Δ::HIS3 ndc80-121/ndc80-125 nuf2-101/NUF2*	This study

[a]All strains have the same markers as W303 except as noted

Table S2 Temperature-sensitive mutants in a lethal insertion cluster identified by linker-scanning mutagenesis

Insertion (first mutation) or Mutation	Sequence[a]	Growth		
		25˚C	30°C	37°C
CGRRQ (Y465C)	TLRQ**CGRRQ**YDSS	++	-	-
CGRKY (D466C)	LRQY**CGRKY**DSSI	+++	+	-
CGRND (S467C)	RQYD**CGRND**SSIQ	+++	+	-
CGRNS (S468C)	QYDS**CGRNS**SIQN	+++	++	-
MRPQS (I469M)	YDSS**MRPQS**IQNL	+++	+++	-
Wild-type	TLRQYDSSIQNL	+++	+++	+++
Y465C	TLRQ**C**DSSIQNL	+++	+++	+++
I469Q	TLRQYDSS**Q**QNL	+++	+++	+++
Y465C I469Q[b]	TLRQ**C**DSS**Q**QNL	+++	+++	-
S467A S468A	TLRQYD**AA**IQNL	+++	+++	+++
S467D S468D	TLRQYD**DD**IQNL	+++	+++	+++
D466G	TLRQY**G**SSIQNL	+++	+++	+++

[a]Insertions and mutations are in bold text
[b]*ndc80-121* allele

Table S3 Immunoprecipitation of Ndc80 complex from wild-type and *ndc80-121* cells

Hit Protein	Wild-type[a]			*ndc80-121*[a]		
	Sequence coverage	Spectrum count (SC)	Normalized SC	Sequence coverage	Spectrum count (SC)	Normalized SC
Ndc80	54%	242	2.18	75%	523	1.10
Spc24	85%	268	2.41	81%	394	0.83
Nuf2-TAP	48%	111	1	57%	475	1
Spc25	50%	92	0.83	55%	284	0.60

[a]Asynchronous cultures were shifted to 37˚C for 100 min. Immunoprecipitated proteins, from a Nuf2-TAP pull-down, were identified by mass spectrometry.

Table S4 Recombinant Ndc80 complex cross-links

Protein 1	Position 1[a]	Protein 2	Position 2[a]	No. PSMs[b]	No. Peptides	Best Peptide *q*-value
Ndc80	1	Ndc80	48	62	1	0
Ndc80	1	Ndc80	67	15	2	0
Ndc80	1	Ndc80	69	7	1	0
Ndc80	1	Ndc80	89	21	1	0
Ndc80	1	Ndc80	122	4	2	0
Ndc80	1	Ndc80	140	11	1	0
Ndc80	1	Ndc80	259	4	1	0.001
Ndc80	1	Ndc80	292	3	1	0
Ndc80	1	Ndc80	305	32	1	0
Ndc80	1	Ndc80	310	6	1	0
Ndc80	1	Ndc80	332	3	1	0
Ndc80	1	Ndc80	338	27	1	0
Ndc80	1	Ndc80	342	1	1	0.008
Ndc80	1	Ndc80	344	14	1	0
Ndc80	1	Ndc80	354	1	1	0.006
Ndc80	1	Ndc80	359	24	1	0
Ndc80	1	Ndc80	370	16	1	0
Ndc80	1	Ndc80	388	2	1	0.001
Ndc80	1	Nuf2	113	3	1	0.004
Ndc80	1	Nuf2	157	19	1	0
Ndc80	1	Nuf2	169	4	1	0
Ndc80	1	Nuf2	200	1	1	0.013
Ndc80	1	Nuf2	220	11	1	0
Ndc80	48	Ndc80	67	21	2	0
Ndc80	48	Ndc80	69	3	1	0.008
Ndc80	48	Ndc80	89	14	1	0
Ndc80	48	Ndc80	122	2	1	0.001
Ndc80	48	Ndc80	138	3	1	0.004
Ndc80	48	Ndc80	140	2	1	0
Ndc80	48	Ndc80	231	5	1	0
Ndc80	48	Ndc80	238	2	1	0.004
Ndc80	48	Ndc80	259	5	1	0
Ndc80	48	Ndc80	292	2	1	0.002
Ndc80	48	Ndc80	305	12	1	0
Ndc80	48	Ndc80	310	1	1	0.043
Ndc80	48	Ndc80	332	1	1	0.005
Ndc80	48	Ndc80	338	12	1	0
Ndc80	48	Ndc80	354	4	1	0.001
Ndc80	48	Ndc80	388	2	1	0.001
Ndc80	48	Nuf2	157	12	1	0
Ndc80	48	Nuf2	169	6	2	0
Ndc80	48	Nuf2	220	1	1	0
Ndc80	48	His_6-Spc24	159	1	1	0.023
Ndc80	48	His_6-Spc24	225	1	1	0.006
Ndc80	67	Ndc80	89	21	2	0
Ndc80	67	Ndc80	122	1	1	0.037
Ndc80	67	Nuf2	157	6	2	0

Protein 1	Position 1[a]	Protein 2	Position 2[a]	No. PSMs[b]	No. Peptides	Best Peptide *q*-value
Ndc80	67	His_6-Spc24	183	2	1	0.004
Ndc80	69	Ndc80	89	5	1	0
Ndc80	69	Ndc80	122	1	1	0.002
Ndc80	69	Ndc80	231	1	1	0.036
Ndc80	69	Nuf2	157	3	1	0.001
Ndc80	89	Ndc80	122	11	2	0
Ndc80	89	Ndc80	138	8	1	0
Ndc80	89	Ndc80	140	2	1	0
Ndc80	89	Ndc80	192	2	1	0.001
Ndc80	89	Ndc80	231	10	2	0
Ndc80	89	Ndc80	238	1	1	0.004
Ndc80	89	Ndc80	259	1	1	0
Ndc80	89	Nuf2	113	4	1	0
Ndc80	89	His_6-Spc24	183	1	1	0.003
Ndc80	122	Ndc80	152	28	4	0
Ndc80	122	Ndc80	155	40	2	0
Ndc80	137	Ndc80	140	18	3	0
Ndc80	140	Ndc80	238	1	1	0.003
Ndc80	259	Ndc80	332	13	1	0
Ndc80	259	Nuf2	169	38	4	0
Ndc80	332	Nuf2	169	3	1	0
Ndc80	342	Nuf2	193	3	1	0.003
Ndc80	344	Ndc80	351	8	1	0.012
Ndc80	344	Ndc80	354	14	1	0.001
Ndc80	344	Nuf2	157	3	1	0.002
Ndc80	344	Nuf2	169	23	4	0
Ndc80	344	Nuf2	187	1	1	0.03
Ndc80	351	Ndc80	359	21	2	0
Ndc80	351	Nuf2	187	62	4	0.001
Ndc80	354	Nuf2	187	52	4	0
Ndc80	359	Ndc80	370	66	2	0
Ndc80	359	Ndc80	388	1	1	0.004
Ndc80	359	Nuf2	157	12	1	0
Ndc80	359	Nuf2	200	20	3	0
Ndc80	359	Nuf2	204	1	1	0
Ndc80	359	Nuf2	217	3	1	0
Ndc80	359	Nuf2	220	7	1	0.001
Ndc80	368	Nuf2	201	2	1	0.003
Ndc80	368	Nuf2	204	40	2	0
Ndc80	370	Nuf2	217	40	2	0.001
Ndc80	370	Nuf2	220	118	2	0
Ndc80	377	Ndc80	388	73	3	0.001
Ndc80	377	Nuf2	220	70	1	0.001
Ndc80	380	Ndc80	388	7	1	0.003
Ndc80	380	Nuf2	220	9	1	0.002
Ndc80	382	Nuf2	220	12	1	0.001
Ndc80	388	Nuf2	220	5	1	0.002
Ndc80	404	Ndc80	409	11	1	0

Protein 1	Position 1[a]	Protein 2	Position 2[a]	No. PSMs[b]	No. Peptides	Best Peptide *q*-value
Ndc80	409	Nuf2	246	5	2	0
Ndc80	409	Nuf2	388	1	1	0.012
Ndc80	425	Ndc80	432	6	2	0.003
Ndc80	432	Nuf2	270	8	1	0.002
Ndc80	432	Nuf2	271	1	1	0.009
Ndc80	439	Ndc80	439	1	1	0.011
Ndc80	439	Ndc80	445	2	1	0.023
Ndc80	445	Ndc80	448	51	3	0
Ndc80	445	Ndc80	456	1	1	0.032
Ndc80	448	Nuf2	366	2	1	0.01
Ndc80	489	Ndc80	513	6	2	0
Ndc80	489	Ndc80	522	1	1	0.003
Ndc80	513	Ndc80	527	8	2	0
Ndc80	522	Ndc80	527	6	1	0.001
Ndc80	527	Ndc80	537	1	1	0.005
Ndc80	537	Ndc80	548	14	1	0.008
Ndc80	541	Nuf2	322	8	2	0
Ndc80	548	Ndc80	554	34	2	0
Ndc80	548	Nuf2	329	1	1	0.004
Ndc80	551	Ndc80	560	2	1	0.009
Ndc80	554	Ndc80	566	1	1	0.004
Ndc80	554	Nuf2	331	205	1	0
Ndc80	554	His_6-Spc24	36	1	1	0.022
Ndc80	577	Nuf2	366	23	4	0
Ndc80	582	Nuf2	356	5	1	0.001
Ndc80	582	Nuf2	360	33	3	0
Ndc80	582	Nuf2	366	6	1	0.001
Ndc80	598	Ndc80	602	15	1	0.001
Ndc80	598	Ndc80	613	1	1	0.02
Ndc80	598	Ndc80	627	2	1	0.013
Ndc80	598	Nuf2	388	6	1	0
Ndc80	598	Nuf2	406	2	1	0.001
Ndc80	602	Ndc80	613	56	3	0
Ndc80	602	Ndc80	627	2	1	0.001
Ndc80	602	Nuf2	388	20	1	0.001
Ndc80	602	Nuf2	390	3	1	0
Ndc80	602	Nuf2	393	12	2	0
Ndc80	602	Nuf2	406	2	1	0
Ndc80	611	Nuf2	382	68	2	0
Ndc80	611	Nuf2	388	13	3	0
Ndc80	611	Nuf2	390	107	4	0
Ndc80	611	Nuf2	393	76	3	0
Ndc80	611	Nuf2	406	3	1	0
Ndc80	611	His_6-Spc24	2	5	1	0
Ndc80	613	Nuf2	388	27	2	0
Ndc80	613	Nuf2	393	4	1	0
Ndc80	613	Nuf2	406	3	1	0.001
Ndc80	627	Ndc80	632	10	1	0

Protein 1	Position 1[a]	Protein 2	Position 2[a]	No. PSMs[b]	No. Peptides	Best Peptide *q*-value
Ndc80	627	Nuf2	406	1	1	0.009
Ndc80	627	Nuf2	409	14	4	0
Ndc80	627	Nuf2	415	76	6	0
Ndc80	627	Nuf2	419	14	1	0.001
Ndc80	627	His_6-Spc24	2	2	1	0
Ndc80	632	Nuf2	406	20	2	0
Ndc80	632	Nuf2	409	30	4	0
Ndc80	632	His_6-Spc24	2	2	1	0.005
Ndc80	632	His_6-Spc24	24	20	1	0
Ndc80	641	His_6-Spc24	24	64	2	0
Ndc80	641	His_6-Spc24	137	3	1	0
Ndc80	655	His_6-Spc24	24	23	1	0
Nuf2	187	Nuf2	201	1	1	0.002
Nuf2	200	Nuf2	204	19	1	0
Nuf2	260	Nuf2	271	11	1	0
Nuf2	322	Nuf2	331	1	1	0
Nuf2	360	Nuf2	366	1	1	0.047
Nuf2	360	Nuf2	375	2	1	0.013
Nuf2	360	Nuf2	393	1	1	0.011
Nuf2	366	Nuf2	375	7	1	0.001
Nuf2	366	Nuf2	419	4	1	0.003
Nuf2	375	Nuf2	393	1	1	0.044
Nuf2	382	Nuf2	393	3	1	0
Nuf2	388	Nuf2	388	1	1	0
Nuf2	388	Nuf2	393	12	2	0
Nuf2	393	His_6-Spc24	2	3	1	0.011
Nuf2	409	His_6-Spc24	2	1	1	0.001
Nuf2	415	Nuf2	426	16	1	0
His_6-Spc24	2	His_6-Spc24	24	50	1	0
His_6-Spc24	2	His_6-Spc24	52	11	1	0
His_6-Spc24	24	His_6-Spc24	52	1	1	0.014
His_6-Spc24	24	His_6-Spc24	118	2	1	0.006
His_6-Spc24	24	His_6-Spc24	143	1	1	0.003
His_6-Spc24	24	His_6-Spc24	183	2	1	0.002
His_6-Spc24	36	His_6-Spc24	62	1	1	0.002
His_6-Spc24	36	His_6-Spc24	118	5	1	0.001
His_6-Spc24	36	His_6-Spc24	225	4	1	0.003
His_6-Spc24	52	His_6-Spc24	62	16	1	0
His_6-Spc24	52	His_6-Spc24	118	1	1	0.009
His_6-Spc24	62	His_6-Spc24	71	7	2	0
His_6-Spc24	62	His_6-Spc24	75	4	1	0.009
His_6-Spc24	62	His_6-Spc24	81	1	1	0.009
His_6-Spc24	62	His_6-Spc24	82	1	1	0.004
His_6-Spc24	62	His_6-Spc24	137	1	1	0.001
His_6-Spc24	62	His_6-Spc24	183	4	1	0.002
His_6-Spc24	62	His_6-Spc24	225	1	1	0.013
His_6-Spc24	71	His_6-Spc24	81	12	1	0.014
His_6-Spc24	71	His_6-Spc24	82	6	1	0.002

Protein 1	Position 1[a]	Protein 2	Position 2[a]	No. PSMs[b]	No. Peptides	Best Peptide *q*-value
His_6-Spc24	71	His_6-Spc24	118	1	1	0.027
His_6-Spc24	71	His_6-Spc24	137	4	1	0.039
His_6-Spc24	75	His_6-Spc24	82	23	1	0.005
His_6-Spc24	82	His_6-Spc24	92	18	2	0
His_6-Spc24	82	His_6-Spc24	110	4	1	0
His_6-Spc24	82	His_6-Spc24	118	4	1	0.002
His_6-Spc24	82	His_6-Spc24	137	6	1	0.004
His_6-Spc24	82	His_6-Spc24	225	5	1	0.01
His_6-Spc24	92	His_6-Spc24	118	5	2	0
His_6-Spc24	92	His_6-Spc24	155	1	1	0.004
His_6-Spc24	92	His_6-Spc24	225	1	1	0.001
His_6-Spc24	110	His_6-Spc24	118	425	1	0
His_6-Spc24	110	His_6-Spc24	137	2	1	0
His_6-Spc24	110	His_6-Spc24	139	6	1	0
His_6-Spc24	110	His_6-Spc24	143	5	1	0
His_6-Spc24	110	His_6-Spc24	155	5	1	0.004
His_6-Spc24	110	His_6-Spc24	204	1	1	0.002
His_6-Spc24	110	His_6-Spc24	225	5	1	0
His_6-Spc24	115	His_6-Spc24	225	1	1	0.001
His_6-Spc24	118	His_6-Spc24	139	4	1	0.016
His_6-Spc24	118	His_6-Spc24	143	6	1	0.001
His_6-Spc24	118	His_6-Spc24	155	11	1	0.002
His_6-Spc24	118	His_6-Spc24	159	6	1	0
His_6-Spc24	118	His_6-Spc24	181	3	1	0.001
His_6-Spc24	118	His_6-Spc24	183	8	1	0.018
His_6-Spc24	118	His_6-Spc24	204	6	1	0
His_6-Spc24	118	His_6-Spc24	223	7	2	0.001
His_6-Spc24	118	His_6-Spc24	225	12	1	0.001
His_6-Spc24	137	His_6-Spc24	143	10	1	0.002
His_6-Spc24	137	His_6-Spc24	155	14	1	0.001
His_6-Spc24	137	His_6-Spc24	159	5	1	0
His_6-Spc24	137	His_6-Spc24	183	7	1	0.017
His_6-Spc24	137	His_6-Spc24	204	2	1	0.005
His_6-Spc24	137	His_6-Spc24	225	5	1	0.003
His_6-Spc24	139	His_6-Spc24	155	10	1	0.002
His_6-Spc24	139	His_6-Spc24	159	12	1	0
His_6-Spc24	139	His_6-Spc24	181	2	1	0.001
His_6-Spc24	139	His_6-Spc24	204	6	1	0
His_6-Spc24	139	His_6-Spc24	223	2	1	0.001
His_6-Spc24	139	His_6-Spc24	225	5	1	0.013
His_6-Spc24	143	His_6-Spc24	159	23	1	0
His_6-Spc24	143	His_6-Spc24	181	1	1	0.001
His_6-Spc24	143	His_6-Spc24	183	19	1	0
His_6-Spc24	143	His_6-Spc24	204	6	1	0
His_6-Spc24	143	His_6-Spc24	223	3	1	0.002
His_6-Spc24	143	His_6-Spc24	225	2	1	0.007
His_6-Spc24	155	His_6-Spc24	159	4	1	0.001
His_6-Spc24	155	His_6-Spc24	181	6	1	0.001

Protein 1	Position 1[a]	Protein 2	Position 2[a]	No. PSMs[b]	No. Peptides	Best Peptide *q*-value
His_6-Spc24	155	His_6-Spc24	183	6	1	0.001
His_6-Spc24	155	His_6-Spc24	204	6	1	0.002
His_6-Spc24	155	His_6-Spc24	223	3	1	0.015
His_6-Spc24	155	His_6-Spc24	225	8	1	0.002
His_6-Spc24	159	His_6-Spc24	159	1	1	0.004
His_6-Spc24	159	His_6-Spc24	183	19	1	0
His_6-Spc24	159	His_6-Spc24	204	7	1	0
His_6-Spc24	159	His_6-Spc24	223	1	1	0
His_6-Spc24	159	His_6-Spc24	225	8	1	0
His_6-Spc24	181	His_6-Spc24	204	5	1	0
His_6-Spc24	181	His_6-Spc24	223	1	1	0.001
His_6-Spc24	181	His_6-Spc24	225	4	1	0
His_6-Spc24	183	His_6-Spc24	204	23	1	0
His_6-Spc24	183	His_6-Spc24	223	4	2	0.002
His_6-Spc24	183	His_6-Spc24	225	15	1	0.007
His_6-Spc24	204	His_6-Spc24	225	11	1	0
His_6-Spc24	223	His_6-Spc24	225	1	1	0.002
His_6-Spc24	225	His_6-Spc24	225	6	1	0.003
Spc25	2	Spc25	19	4	1	0
Spc25	2	Ndc80	641	37	1	0
Spc25	2	His_6-Spc24	2	15	1	0
Spc25	19	Ndc80	655	36	3	0
Spc25	19	His_6-Spc24	2	23	1	0.001
Spc25	118	Spc25	118	5	1	0
Spc25	118	Ndc80	48	4	1	0
Spc25	118	Ndc80	89	4	1	0
Spc25	118	His_6-Spc24	110	3	1	0
Spc25	118	His_6-Spc24	118	3	1	0.002
Spc25	118	His_6-Spc24	137	15	1	0
Spc25	118	His_6-Spc24	139	8	1	0.004
Spc25	118	His_6-Spc24	143	25	1	0
Spc25	118	His_6-Spc24	155	17	1	0.001
Spc25	118	His_6-Spc24	159	19	1	0
Spc25	118	His_6-Spc24	181	1	1	0.002
Spc25	118	His_6-Spc24	183	10	1	0.004
Spc25	118	His_6-Spc24	204	13	1	0
Spc25	118	His_6-Spc24	223	4	2	0.001
Spc25	118	His_6-Spc24	225	8	1	0

[a]Wild-type sequence of Spc24 starts at residue 21 due to presence of His_6 tag
[b]PSM, peptide spectrum match

Table S5 Recombinant Ndc80 complex loop-links

Protein	Position 1[a]	Position 2[a]	No. PSMs[b]	No. Peptides	Best Peptide *q*-value
Ndc80	67	69	19	1	0
Ndc80	137	138	41	4	0
Ndc80	137	140	8	2	0
Ndc80	138	140	18	2	0
Ndc80	152	155	25	2	0
Ndc80	332	338	6	1	0
Ndc80	338	342	20	3	0
Ndc80	342	344	7	1	0.002
Ndc80	349	351	3	2	0.002
Ndc80	351	354	37	6	0
Ndc80	354	359	14	2	0
Ndc80	359	368	4	2	0.002
Ndc80	359	370	8	2	0.002
Ndc80	368	370	2	1	0
Ndc80	370	377	8	1	0.002
Ndc80	377	380	32	1	0.001
Ndc80	380	382	2	1	0.001
Ndc80	382	388	7	1	0
Ndc80	382	393	1	1	0.002
Ndc80	388	393	1	1	0.001
Ndc80	393	404	28	3	0
Ndc80	404	408	20	1	0
Ndc80	408	409	24	1	0
Ndc80	432	439	1	1	0.001
Ndc80	439	445	14	2	0
Ndc80	445	448	15	3	0
Ndc80	448	456	7	1	0
Ndc80	513	522	8	1	0
Ndc80	513	523	9	1	0
Ndc80	522	523	14	3	0
Ndc80	522	527	1	1	0.001
Ndc80	523	527	20	1	0
Ndc80	537	541	5	1	0.001
Ndc80	537	548	1	1	0.023
Ndc80	541	548	3	2	0.001
Ndc80	548	551	26	4	0
Ndc80	548	554	2	2	0.001
Ndc80	551	554	60	4	0
Ndc80	554	560	6	1	0
Ndc80	560	566	9	3	0
Ndc80	566	577	4	1	0.002
Ndc80	598	601	18	2	0
Ndc80	601	602	12	2	0
Ndc80	602	611	1	1	0.002
Ndc80	602	613	2	2	0.002
Ndc80	611	613	12	3	0
Ndc80	638	641	60	1	0

Protein	Position 1[a]	Position 2[a]	No. PSMs[b]	No. Peptides	Best Peptide *q*-value
Nuf2	187	193	2	1	0.005
Nuf2	193	200	30	1	0
Nuf2	200	201	62	3	0
Nuf2	200	204	1	1	0.002
Nuf2	201	204	23	1	0
Nuf2	217	220	97	1	0
Nuf2	220	225	3	1	0
Nuf2	243	246	76	3	0
Nuf2	270	271	7	1	0
Nuf2	322	329	52	2	0
Nuf2	356	360	48	2	0
Nuf2	360	366	1	1	0.001
Nuf2	375	382	24	1	0
Nuf2	382	388	12	2	0
Nuf2	382	390	13	2	0
Nuf2	382	393	3	1	0.001
Nuf2	388	390	112	3	0
Nuf2	388	393	18	2	0
Nuf2	390	393	96	2	0
Nuf2	406	409	39	2	0
Nuf2	409	415	1	1	0.003
Nuf2	415	419	39	2	0
Nuf2	419	426	15	1	0
His_6-Spc24	71	75	26	2	0
His_6-Spc24	75	81	3	2	0.002
His_6-Spc24	75	82	2	1	0.004
His_6-Spc24	81	82	15	2	0
His_6-Spc24	92	110	10	2	0.001
His_6-Spc24	110	115	20	2	0
His_6-Spc24	110	118	21	1	0
His_6-Spc24	115	118	30	2	0
His_6-Spc24	137	139	13	2	0
His_6-Spc24	137	143	8	1	0
His_6-Spc24	139	143	33	1	0
His_6-Spc24	155	157	22	3	0
His_6-Spc24	157	159	33	1	0
His_6-Spc24	181	183	18	1	0
His_6-Spc24	223	225	17	2	0

[a]Wild-type sequence of Spc24 starts at residue 21 due to presence of His_6 tag
[b]PSM, peptide spectrum match

Literature Cited

GEISER, J. R., H. A. SUNDBERG, B. H. CHANG, E. G. MULLER and T. N. DAVIS, 1993 The essential mitotic target of calmodulin is the 110-kilodalton component of the spindle pole body in Saccharomyces cerevisiae. Mol Cell Biol **13:** 7913-7924.

GREENLAND, K. B., H. DING, M. COSTANZO, C. BOONE and T. N. DAVIS, 2010 Identification of Saccharomyces cerevisiae spindle pole body remodeling factors. PLoS One **5:** e15426.

MCDONNELL, A. V., T. JIANG, A. E. KEATING and B. BERGER, 2006 Paircoil2: improved prediction of coiled coils from sequence. Bioinformatics **22:** 356-358.

WARGACKI, M. M., J. C. TAY, E. G. MULLER, C. L. ASBURY and T. N. DAVIS, 2010 Kip3, the yeast kinesin-8, is required for clustering of kinetochores at metaphase. Cell Cycle **9:** 2581-2588.